ADAPTIVE OFDM-BASED ACOUSTIC UNDERWATER TRANSMISSION: SYSTEM DESIGN AND EXPERIMENTAL VERIFICATION

A Thesis

by

Mohammad Sadeghi

Submitted to the
Graduate School of Sciences and Engineering
In Partial Fulfillment of the Requirements for
the Degree of

Master of Science

in the
Department of Electrical and Electronics Engineering

Özyeğin University
August 2017

ADAPTIVE OFDM-BASED ACOUSTIC UNDERWATER TRANSMISSION: SYSTEM DESIGN AND EXPERIMENTAL VERIFICATION

Approved by:

Professor Murat Uysal, Advisor
Department of Electrical and Electronics Engineering
Özyeğin University

Asst.Prof. Kadir Durak
Department of Electrical and Electronics Engineering
Özyeğin University

Asst.Prof. Tuncer Baykas
Department of Computer Engineering
Medipol University

Date Approved: August 2017

This thesis is dedicated to my beloved parents, Zamzam and Abdolah, for their love, endless support and encouragement.

ABSTRACT

In this study, we design and implement an adaptive Underwater Acoustic (UWA) orthogonal frequency division multiplexing (OFDM) system employing adaptive modulation and transmit power. Recently, UWA communications gain more attractions as there has been a growing interest in exploring the communications possibilities for underwater applications such as oil field monitoring, oceanographic data collection, maritime archaeology and disaster prevention. However, the harsh characteristic of underwater environments imposes various difficulties for communication in this medium. Thus, proposing a reliable UWA communication system which has a high data rate can improve these applications performance significantly.

Since UWA communications suffer from low data rates, we propose an adaptive OFDM communication system to support higher data rates over UWA channel. OFDM is an attractive technique for underwater channels due to the fact that inter-symbol-interference resulted from frequency selective channels can be removed completely. Additionally, adaptive communications achieve significant improvements in transmission data rate. For the sake of implementation, we take advantages of LabVIEW software to generate OFDM blocks. The generated data is transmitted to the receiver side with the aid of Software defined radios (USRPs) and acoustic front-ends. The received data at the acoustic hydrophones are transferred to the USRPs and then processed in LabVIEW for information detection. We conduct our experiments at the pool to investigate the performance of the proposed system over a real UWA channel.

ÖZETÇE

Bu çalışmada, adaptif kipleme ve verici gücü kullanan bir adaptif Sualtı Akustik (Underwater Acoustic - UWA) dik frekans bölmeli çoğullama (Orthogonal Frequency Division Multiplexing - OFDM) sistemi tasarladık ve gerçekledik. Son zamanlarda, petrol yatağı görüntüleme, oşinografik veri toplama, deniz arkeolojisi, ve afet önleme gibi uygulamalar için haberleşme imkanları keşvetmeye yönelik artan bir ilgi olduğundan, UWA haberleşmesi daha fazla cazibe toplamaktadır. Ancak, sualtı ortamlarının sert karakteristikleri, bu ortamda haberleşme yapmanın önüne çeşitli zorluklar çıkarmaktadır. Dolayısıyla, yüksek veri hızına sahip güvenilir bir UWA haberleşme sistemi ortaya çıkarmak, bu uygulamaların performansını önemli ölçüde arttırabilir.

UWA haberleşmesi, düşük veri hızlarından müzdarip olduğundan, UWA kanalında yüksek hızları desteklemek için adaptif bir OFDM haberleşme sistemi öne sürüyoruz. OFDM, frekans seçici kanallardan kaynaklı simgelerarası girişiminden tamamen kurtulmayı sağlaması sebebiyle, sualtı kanalları için çekici bir tekniktir. Ek olarak, adaptif haberleşme, veri iletim hızında önemli iyileştirmeler sağlayabilmektedir. Gerçekleme adına, OFDM bloklarını üretmek için LabVIEW yazılımını kullandık. Üretilen veri, alıcı tarafına Yazılım Tabanlı Radyo (USRP) yardımıyla ve akustik ön uçlar ile iletildi. Akustik hidrofonlarda alınan veri, USRP'lere iletildi ve bilgiyi elde etmek üzere LabVIEW ile işlendi. Öne sürdüğümüz sistemin performansını gerçek bir UWA kanalında test etmek için deneylerimizi bir havuzda gerçekleştirdik.

ACKNOWLEDGEMENTS

I would like to thank all those people without whom it would not be possible to complete this thesis.

Foremost, my sincere gratitude and deepest appreciation go to my supervisor, Professor Murat Uysal. It is hard to find words to describe how much I appreciate all he has done for me as a supervisor. His insightful suggestions, fruitful discussions, kindness, and patience have motivated me throughout my M.Sc. studies.

It is my pleasure to thank the members of my thesis defence committee, Professors Tuncer Baykas and Kadir Durak, for their valuable time in evaluating this thesis.

I am also thankful to my colleague, Mohammed Elamassie, for all his cooperation, assistance and insightful advices.

I am truly grateful to Graduate School of Ozyegin University, and Scientific and Technological Research Council of Turkey (TUBITAK) for awarding me generous scholarships and their consistent support during my M.Sc. studies.

Last, but not the least, my heartiest thanks go to my parents, Zamzam and Abdolah, for their love, endless support and encouragement that helped me to overcome difficulties throughout my life. Without them, nothing would have been possible.

TABLE OF CONTENTS

LIST OF TABLES

LIST OF FIGURES

CHAPTER I

INTRODUCTION

Oceans cover most of the Earths surface. In order to explore this environment, we have to use wireless communication in underwater environment. However, not all of the propagation technologies are suitable for underwater. RF waves are not suitable, since, these waves cannot propagate well through water due to the high attenuation. Optical communications offer low delay but require alignment of transmitter and receiver and also affected by absorption, scattering, and high level of ambient light limiting the transmission ranges. Therefore, in most cases, the only choice is acoustic propagation, which suffers from slow propagation that results in a frequency selective channel. OFDM is a proper choice for underwater acoustic (UWA) channels, since inter-symbol-interference (ISI) resulted from frequency selective channel can be removed completely.

Emerging underwater applications such as offshore oil field exploration/monitoring, oceanographic data collection, maritime archaeology, environmental monitoring, disaster prevention, port security etc. and also limited bandwidth impose further requirements on UWA system design. To support higher data rates over UWA channel, adaptive modulation and transmit power schemes can be employed. The objective of this thesis is to design an adaptive OFDM underwater acoustic system and conduct real time experiments.

1.1 Literature overview

Underwater acoustic first time was employed during World War I to design sonars for detecting obstacles for navigation purposes and locationing the targets. UWA was later used in second World War by U.S. Navy for communicating with submarines and

until 1980s, UWA were mainly employed in military applications. Advancement of DSP and large scale VLSI technologies led to new generations of digital UWA systems were developed for a different civilian purposes [1]. At the time, the modulation choice for UWA acoustic modems was frequency shift keying (FSK) which suffers from bandwidth inefficiency.

In 1994, Stojanovic designed phase-coherent UWA system with joint carrier synchronization and equalization. The receiver employes a decision feedback equalizer (DFE) to reduce the complexity the estimator. After this breakthrough, there was a great attention to coherent phase UWA systems. Researchers has been particularly interested to propose simple equalizers such as sparse channel estimation/equalization and turbo equalization [2] and the references therein.

The emergence of high data rate applications urge more requirements the design of UWA systems. To satisfy such requirements, multiple-input multiple-output (MIMO) whcih result in significant improvement in throughput has been implemented in UWA systems. In [3], the space time trellis coding has been investigated in UWA systems. Simulations/experiments have shown huge improvements in data rate comparing to single-input single-output (SISO) systems. The examples of MIMO single carrier transmissions include the multi channel DFE algorithms in [4, 5, 6, 7], time-reversal combined with single channel DFE in [8, 9, 10, 11], frequency domain equalizers in [12, 13], successive interference cancellation [14, 15], and turbo equalization in [16, 17, 18, 19, 20]. Although MIMO systems result in a higher data rates, their practical implementation over frequency-selective channels particularly UWA channels is challenging. This has lightened interest in combination of MIMO and OFDM for the UWA channel and investigated extensively in recent literature. approaches include the block-by-block receiver design in [21, 22, 23] and the adaptive receiver in [24, 25]. OFDM is particularly attractive for UWA channels due to the fact that channel distortion can be vanished at the receiver on a subcarrier-by-subcarrier basis

and therefore a complex equalizers in time domain is not needed.

1.2 Organization of thesis

The chapters of this thesis are arranged in the following order:

In the second chapter, first, we briefly introduce underwater channel characteristics and then, simulation of an OFDM UWA communication system is presented.

In the third chapter, we provide LabVIEW implementation of the single-input single-output (SISO) OFDM system on software defined radio (USRP) platform. We integrate our USRP system to the acoustic front-end and conduct the experiments in the pool facility.

In the fourth chapter, we simulate and practically implement adaptive OFDM schemes where modulation size/type and transmit power are chosen as adaptive parameters. The aim is to maximize throughput by assigning different modulation size/type and transmit power to each subcarrier while keeping the average BER at a fixed value. We consider three different adaptive schemes. In the first and the second scheme, bit allocation (through the choice of proper modulation type/size) is made adaptively to each subcarrier and the power is equally distributed among subcarriers. The third scheme allocates both modulation and power adaptively based on the channel state information (CSI) at the subcarrier provided by feedback received at the transmitter side. .

Finally the thesis is concluded in the fifth chapter.

CHAPTER II

SIMULATION OF OFDM UWA COMMUNICATION SYSTEM

In this chapter , first, we present a brief explanation of the UWA channel characteristics, including path loss, fading and ambient noise which is critical in the design and evaluation of the system. We then introduce an OFDM system for UWA and we check the efficiency of this system with simulations.

2.1 Channel model

In this section, the characteristics of the UWA channel is discussed, considering the major differences and similarities with RF channel models.

2.1.1 Large-scale path loss

The path loss in UWA channel is due to absorption and spreading losses.

Spreading loss: the decrease of wave energy per unit surface as acoustic signal propagates away from its source [26].

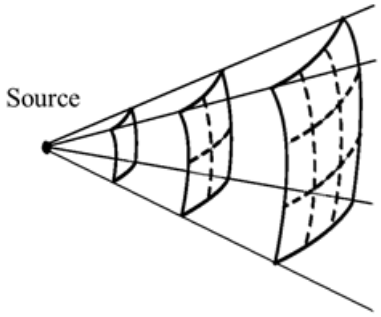

Figure 1: Spreading loss

There are three types of spreading as follows:

Spherical spreading: the uinform decrease of wave energy level in all direction as sound wave propagates away from a source. Cylindrical Spreading: beyond some range the sound cannot propagate uniformly in all directions and hits the sea surface or sea floor. An approximation for spreading loss can be achieved assuming the sound is distributed uniformly over the surface of a cylinder. Practical Spreading: in practice in mid ocean, wave Spreading gradually changes from spherical distribution to cylindrical distribution as shown in fig. 2. Thus, spreading factor of 1.5 is chooses as indicative of practical spreading which is between spreading factor of 2 for spherical spreading and spreading factor of 1 for cylindrical Spreading.

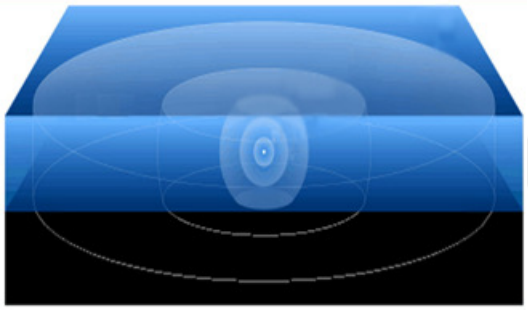

Figure 2: Practical spreading of acoustic waves underwater

Absorption loss: portions of Signal energy changes into heat in the water due to many materials; the absorption of these materials is a function of frequency as well as pressure, temperature, salinity and acidity [27]. Most of energy is being absorbed by the following three materials: pure water Viscosity (H2O), magnesium sulphate (MgSO4) and boric acid (B(OH)3) relaxation. Therefore, total absorption is obtained as follows:

$$\alpha = \alpha_{\mathrm{H_2O}} + \alpha_{\mathrm{MgSO_4}} + \alpha_{\mathrm{B(OH)_3}} \tag{1}$$

The overall path loss is a function of the previous two factors (Spreading loss, k, Absorption loss, α) and a function of distance between source and destination (l):

$$P(f,d) = l^S a(f)^l \tag{2}$$

$$\begin{aligned}[P(f,l)]_{dB} &= 10 \times \log_{10}\left(l^k a(f)^l\right) = 10 \times \log_{10}\left(l^k\right) + 10 \times \log_{10}\left(a(f)^l\right) \\ [P(f,l)]_{dB} &= 10k \times \log_{10}(l) + 10l \times \log_{10}\left(a(f)^l\right)\end{aligned} \tag{3}$$

It should be noticed that overall path loss is an increasing function with distance and frequencies considering all other factors are constants as shown in fig. 3. Several formulas have been developed for the characterization of the absorption coefficient including , Schulkin-Marsh, Fisher-Simmons, Mellen-Browning and Francois-Garrison. Table. 1 [28]:

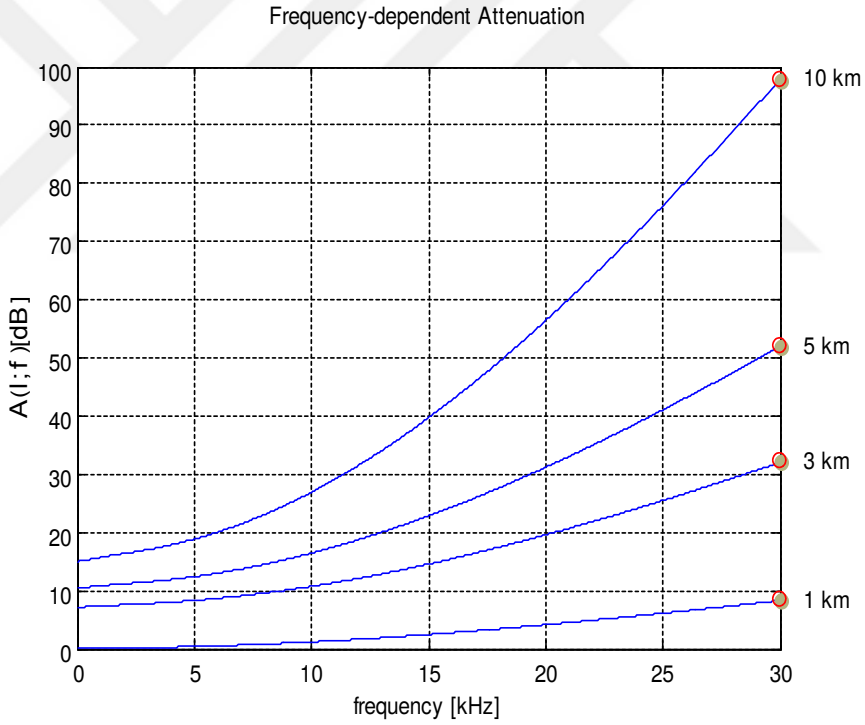

Figure 3: Overall path loss with respect to frequencies at different distances

Thorp's formula is widely employed in the literature due to simplicity. However, this formula is just a function of frequency and ignores other parameters of the UWA channel. The most comprehensive formula pf the the absorption coefficient is Francois- Garrison's (FG) which applies for the frequency range of $200Hz - 1MHz$.

Table 1: Models for absorption factor

Name	Frequency-range	Related parameters
Schulkin-Marsh	2 kHz - 25 kHz	Frequency, temperature,salinity, and pressure
Thorp	100 Hz less than 10 kHz	Frequency
Mellen-Browning	¡ 10 kHz	Frequency
Fisher-Simmons	10 kHz - 400 kHz	Frequency, temperature, and pressure
Francois-Garrison	200 Hz - 1 MHz	Frequency, temperature, salinity, depth, and acidity

This empirical formula is verified with measurements from various oceans and compared further with Schulkin-Marsh and Fisher-Simmons at different frequencies. It is observed that for above 10 kHz their formula tends to Fisher-Simmons equation more than Schulkin-Marsh equation with maximum difference of 20 percent. It has better agreement with Schulkin-Marsh in the range below 1 kHz in warm waters. Under specific conditions it tends to Thorps formula in above 1 kHz as shown in fig. 4 [27].

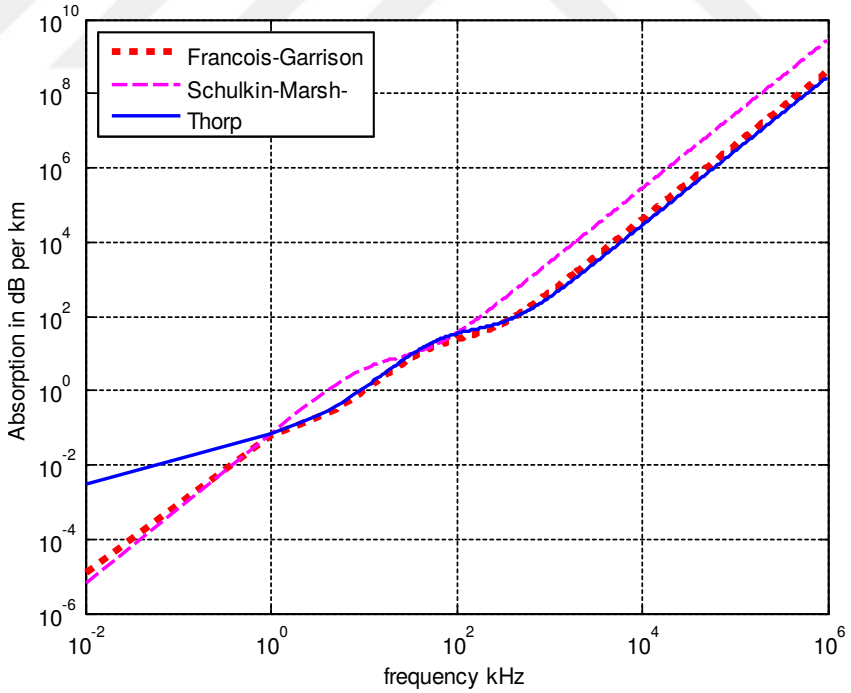

Figure 4: Thorps formula Vs. FG formula and Schulkin-Marsh formula

2.1.2 Small-scale fading

It is used to describe the rapid fluctuations of the amplitudes, phases, or multipath delays of a wave in a short period of time [29]. In an Underwater environments we have two main reasons for Fading depend on the depth of water.

Shallow water: it is primarily results from the signals reflected from the surface, bottom, and other objects in the water as shown in fig. 5.

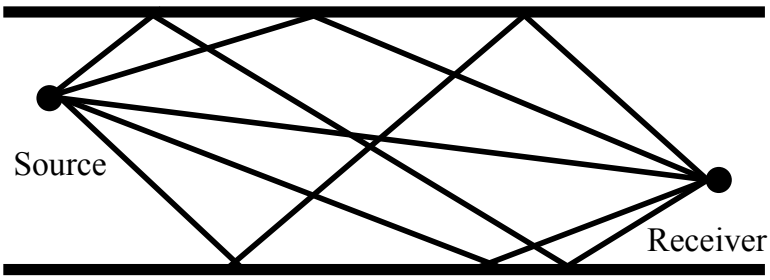

Figure 5: Multipath waves in shallow water

In deep water: it is primarily due to a phenomenon known as ray bending, i.e., the tendency of acoustic waves to travel along the axis of lowest sound speed as shown in fig. 6.

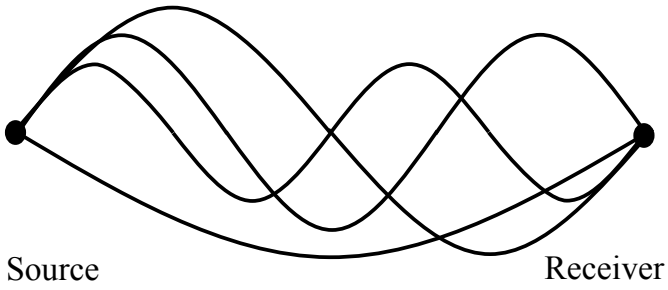

Figure 6: Multipath waves in deep water

This results in a selective channel model in frequency domain where each frequency components of the transmitted signal faces different attenuations. The sound speed in underwater environment is about 1500 m/s. This slow speed leads to delay spreads of

order 10-100 milliseconds. The UWA channel has sparse channel characteristics.Thus the channel impulse response of UWA includes a large number of zero taps because the energy of channel is mostly localized around small ranges of delays.

Experimental results of UWA channel impulse response suggest that OFDM is an attractive method for communication over underwater acoustic sparse frequency-selective channels. VHF08 experiment: the VHF08 experiment as shown in fig. 7 was hold in April 2008 in Buzzards Bay . The water depth was 12 m. Two transmitters were submerged 6 m below a surface buoy. The receiving array was about 6 m below a boat. The transmission distance was 450 m [23].

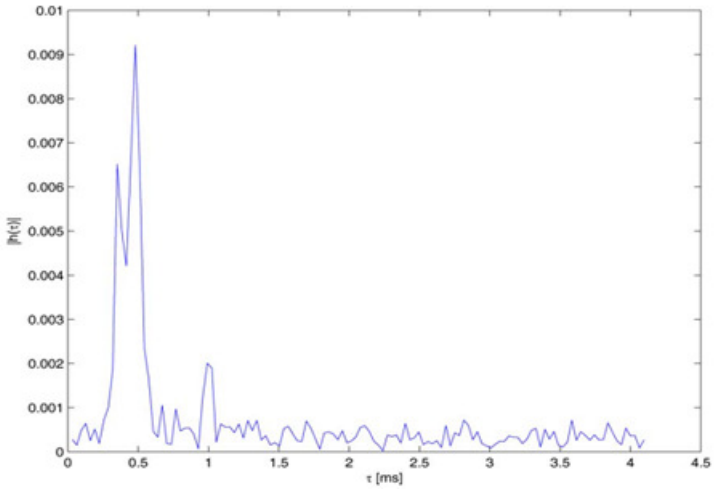

Figure 7: Estimated channel of VHF08 scenario for one OFDM block

AUV07 experiment: the AUV07 experiment as shown in fig. 8 was hold in June 2007 in Panama City. The depth of water was 20 m. Two transmitters were submerged 9 m below a surface buoy. The receiver array was 9 m below a boat. The transmission distances was 500 m [23].

Experimental results shows that some channels may just be characterized as deterministic, while others may exhibit Rice, Rayleigh fading [30, 31], K-distributed [32] and Chi-square distributed [33] in other environments.

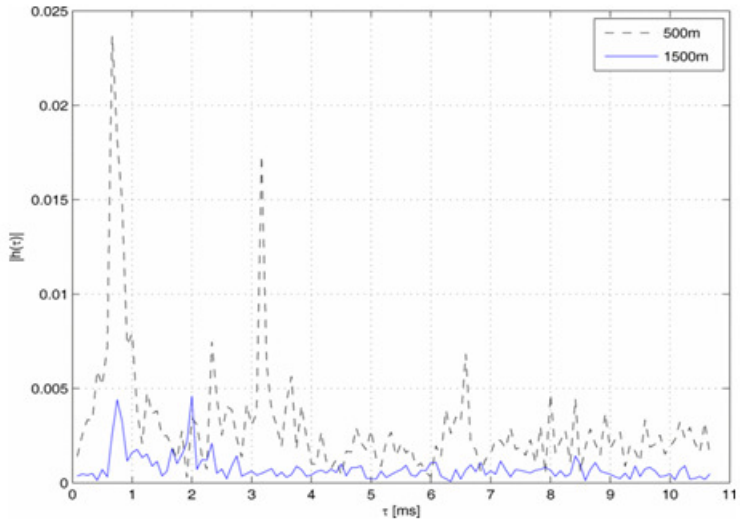

Figure 8: Estimated channel of AUV07 scenario for one OFDM block.

2.1.3 Ambient noise

It is the noise present everywhere in the sea. In order to model the ambient noise, we assume a coloured Gaussian noise. The power spectral density of the ambient noise decreases with frequency. There are many sources of noise in underwater channel such as turbulence, marine life, breaking waves, passing ships, rain, bubbles, and winds, but mainly as shown in fig. 9 it is due to four types and at specific frequency rang it is mainly due to one of the following Noises [34]:

Turbulence: in the frequency range below 10 Hz, the dominant source of the noise is turbulence in the ocean and atmosphere.

Shipping activity: in the frequency range between 10- 100 Hz, noise caused by distant ship traffic is the main source of the noise and modelled by shipping activity factor s, which takes values between 0 and 1.

Surface motion: the main source of surface motion is wind; therefore the wind speed is an important factor in waves noise in the frequency range of 100 Hz-100 kHz. The power spectral density of waves noise can increase more significantly when the wind speed reach from calm to 10 m/s.

Thermal noise: the dominant factor in the frequencies above 100 kHz is thermal noise which results from the molecular motion in the sea.

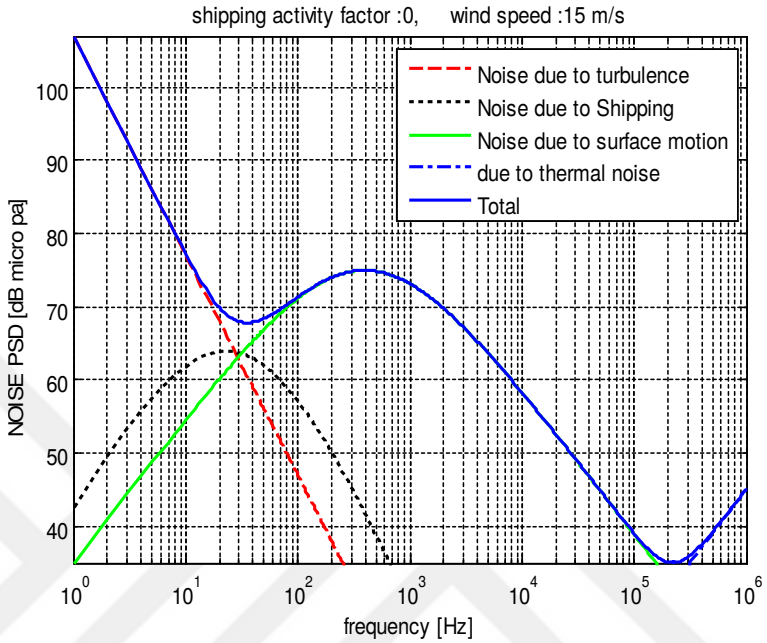

Figure 9: Power Spectral Density of ambient noise

From Total PSD of Noise and PSD of the main four types of Noises, we can notice that the major contributing noise in the range 100 Hz to 100 kHz is surface motion and its Linear in dB and decreasing with frequency. Therefore, it can be approximated easily as follow [28] (the approximation with all PSD of noise are shown in Fig. 10):

$$\begin{aligned} N(f) &= N_t(f) + N_s(f) + N_w(f) + N_{th}(f) \\ N(f) &= \approx N_w(f) = \frac{10^{5+0.75\sqrt{W}} f^2}{(f+f_o)^4} \approx \frac{10^{5+0.75\sqrt{W}}}{f^2} \end{aligned} \tag{4}$$

Signal to Noise Ratio (SNR): SNR is not actually a ratio but the difference in decibels between the power of received signal and power spectral density of noise [41].

$$SNR = \frac{\text{Received Power}}{\text{Noise Power}} = \frac{P/A(l,f)}{N(f)\Delta f} \tag{5}$$

Overall path loss is an increasing function of distance and frequency. Since $A(l,f)$ is an increasing function with frequency, $N(f)$ is a decreasing function with frequency,

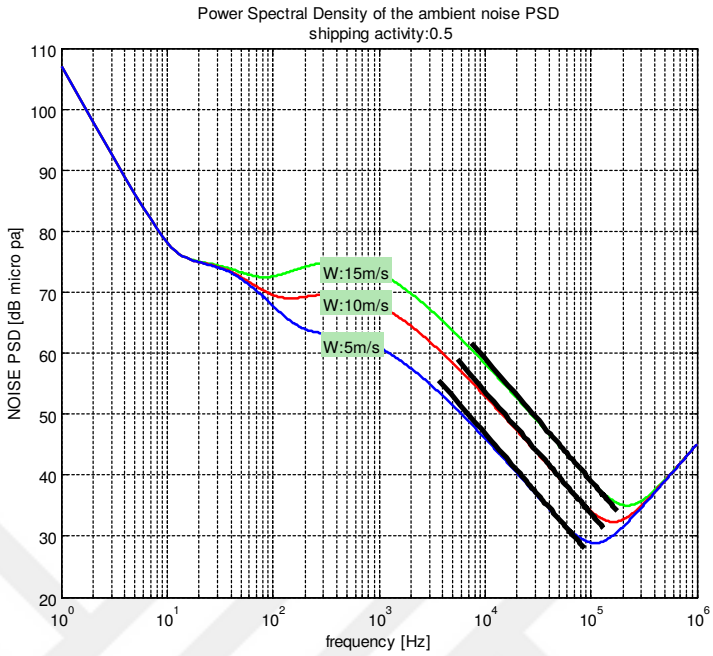

Figure 10: Approximation of PSD of Noise

thus; there is an optimal frequency that can decrease $A(l,f)N(f)$ (increase $\frac{1}{A(l,f)N(f)}$) at specific distance as shown in fig. 11 and fig. 12.

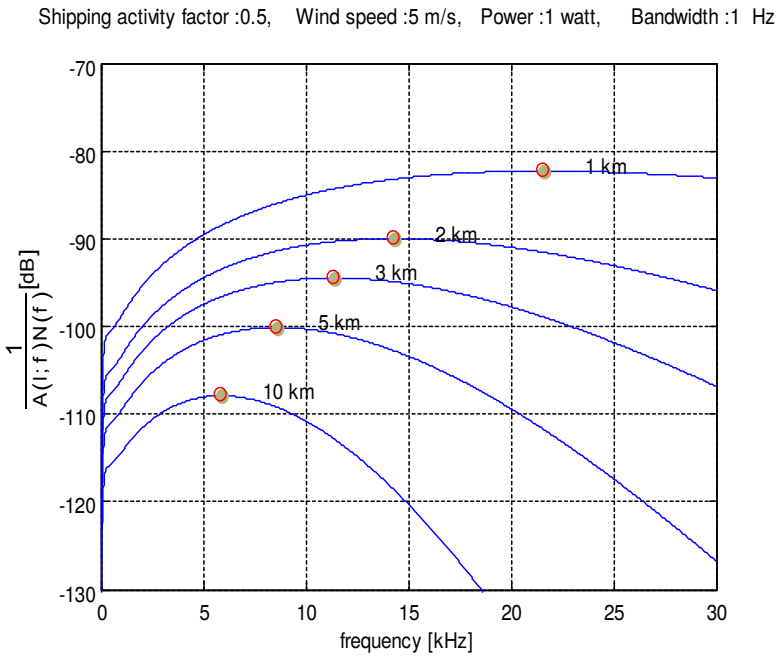

Figure 11: SNR as a function of frequency

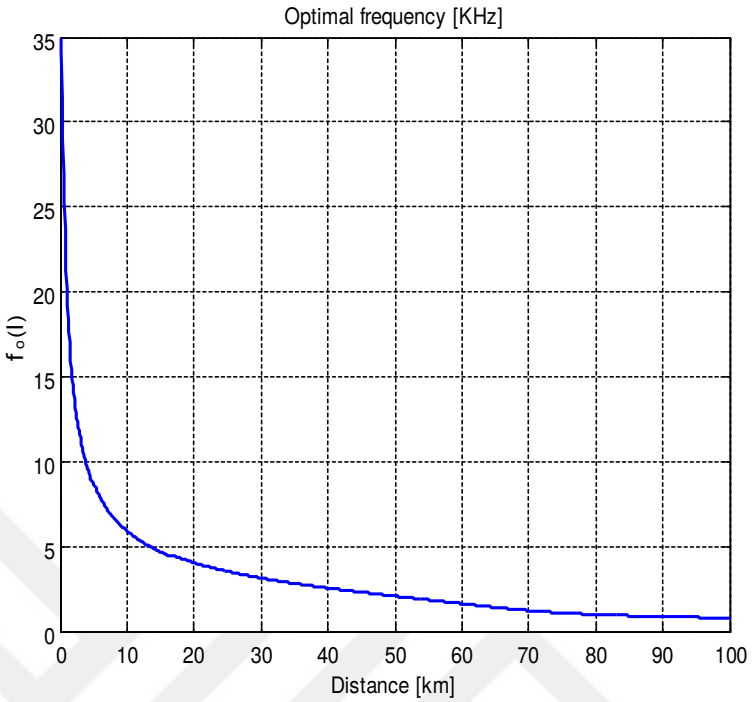

Figure 12: Optimal frequency

2.2 System model

The OFDM overview of the considered system is shown in Fig. 13. The input bit stream is first mapped to the modulation symbols, then K-point IFFT is applied and a CP is appended to eliminate the ISI caused by multipath effect. Additionally, the data stream is convolved with pulse shape filter and then passed through UWA channel. At the receiver, each OFDM frame is then partitioned into individual OFDM symbols. After CP elimination, the resulting sequence is applied to FFT. Afterwards, one tap equalizer are performed. Finally, the equalized data symbols are demodulated and the information data is recovered (details about OFDM implementation are provided in chapter 3)

2.3 Simulation results

In this section, we present numerical results on the BER performance of an OFDM systems over sparse Rayleigh distributed with decaying power profile channel. The

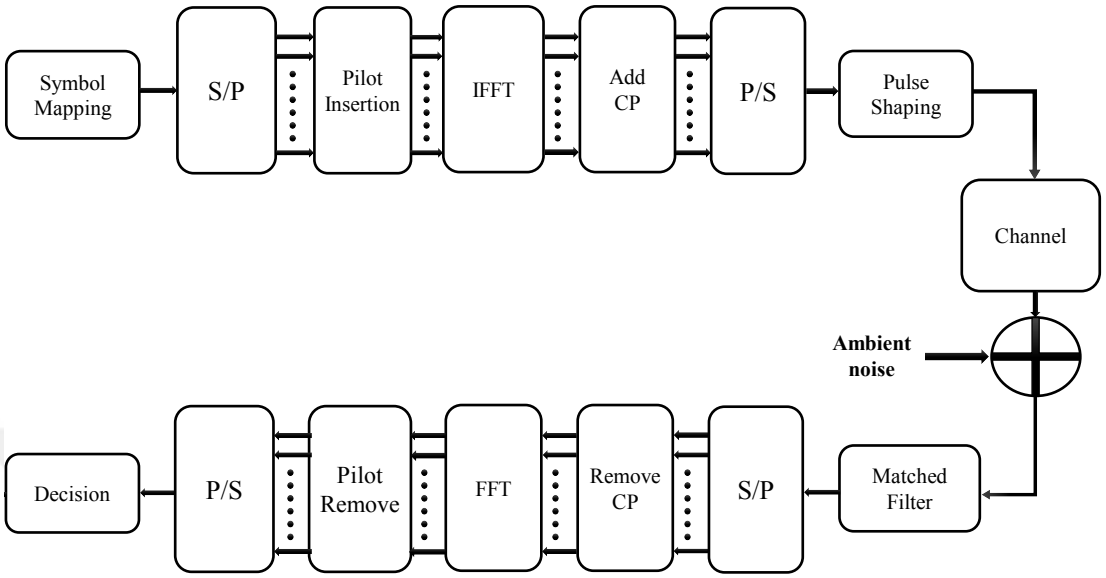

Figure 13: Block diagram of simulated OFDM system

simulation parameters are summarized in table 2.

Table 2: Simulation parameters

Parameters	values
Number of Subcarriers	$K = 1024$
OFDM block duration	$T = 85.33ms$
Guard interval	$T_g = 10ms$
Signal Bandwidth	$B = 12kHz$
Modulation	BPSK/QPSK/8PSK
Pulse shaping	Raised-Cosine ($\beta = 0.5$)

It should be noticed that the number of subcarriers is $K = B \times T = 85.33ms \times 12KHz = 1023.96 \approx 1024$ and the number of cyclic prefix samples: $B \times T_g = 10ms \times 12KHz = 120$. Thorp model is chosen as an attenuation model and Spreading factor is considered as $k = 1.5$ which reasonable for practical system to model the path-loss. Coloured Gaussian noise is considered with PSD defined as:

$$N(f) = \frac{10^{5+0.75\sqrt{W}} f^2}{(f+f_o)^4} \approx \frac{10^{5+0.75\sqrt{W}}}{f^2} \tag{6}$$

Finally sparse Rayleigh distributed with decaying power profile considered as Fading channel model. A sample of simulated channel impulse response is illustrated in fig. 14.

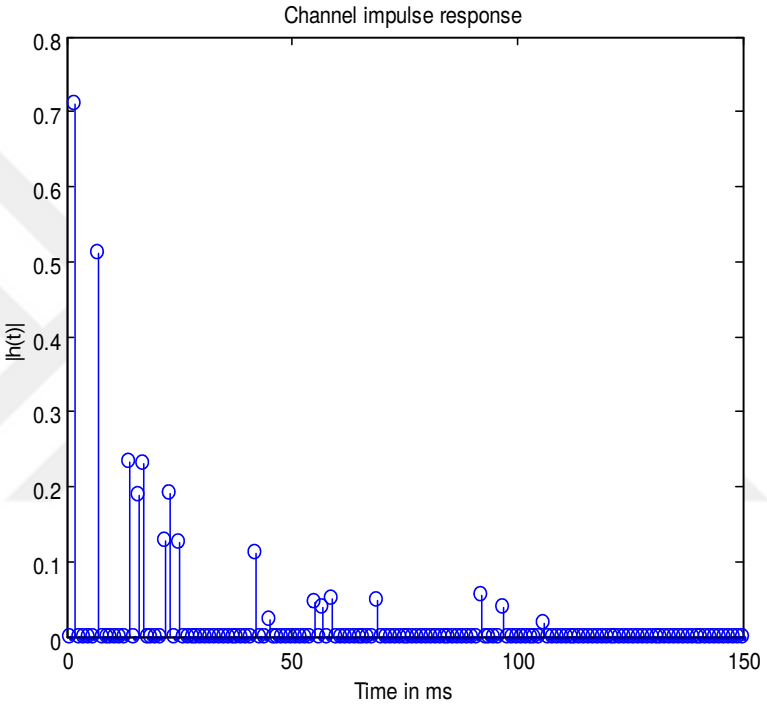

Figure 14: Channel impulse response

In Fig. 15, to evaluate the effect of frequency, BER performance is plotted versus SNR for two set of different distances. It can be observed as it is mentioned in section III, there is an optimal frequency for each distance. Therefore, increasing or decreasing the frequency result in the performance loss.

In Fig. 16, to evaluate the effect of distance, BER performance is plotted versus SNR for different distances ($l = 1,\ 2\,\text{and}\,3\text{km}$) at frequency of $f = 20KHz$. As it is mentioned in section III, the optimal frequency for $l = 1km$ is $20kHz$. Therefore, increasing the link distance results in the performance loss.

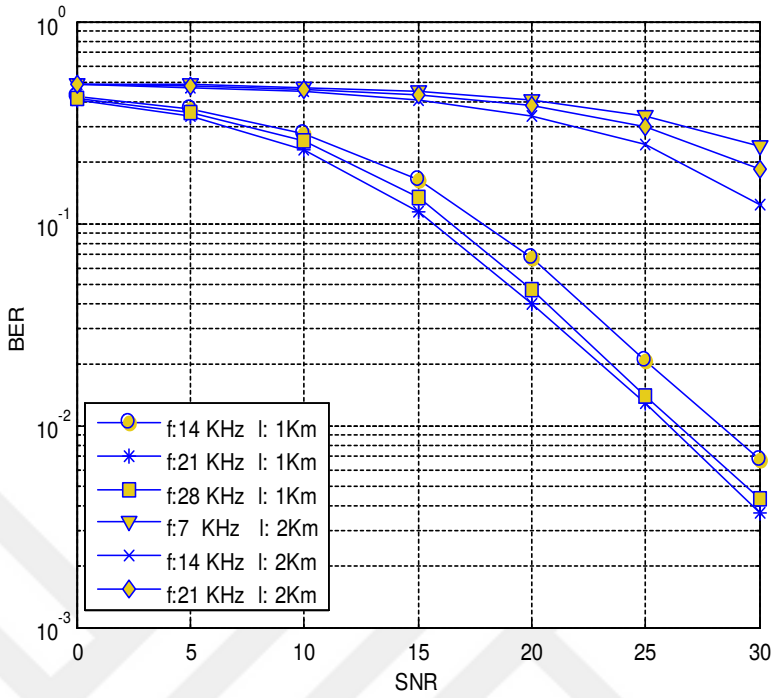

Figure 15: Evaluating the effect of frequency on BER performance

In Fig. 17, we present BER performance for different PSK modulation types at distance of $l = 1km$ and $f = 20KHz$. It can be observed that increasing modulation order degrades performance while it increases spectral efficiency, i.e., 8-PSK carries more bits than 4-PSK and 4-PSK carries more bits than 2-PSK.

Fig. 18 shows the effect of sampling offset on BER performance. Simulation is done for the distance of $l = 1km$ and $f = 20KHz$. It can be noticed that sampling offset (where time samples are taken) degrades the system performance. Therefore offset correction should be made in practical implementation.

Fig. 19 shows the effect of frequency offset on BER performance. Simulation is done for the distance of $l = 1km$ and $f = 20KHz$. It can be noticed that carrier frequency offset (CFO) dramatically degrades the system performance since CFO destructs the orthogonality between subcarriers. CFO compensation should be made in practical implementation.

In Fig. 20 to evaluate the effect coloured Gaussian noise, we compare the BER

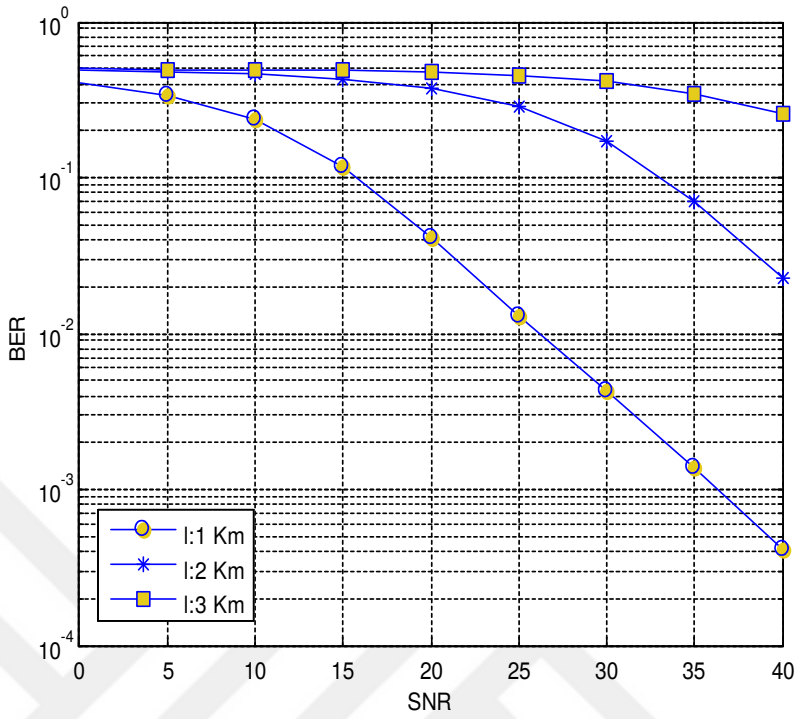

Figure 16: Evaluating the effect of link distance on BER performance

performance of OFDM system in the presence of white Gaussian noise and coloured Gaussian noise. It can be observed that coloured noise results in great degradation in performance with respect to white noise. Therefore, the effect of coloured noise could be removed using whitening filter.

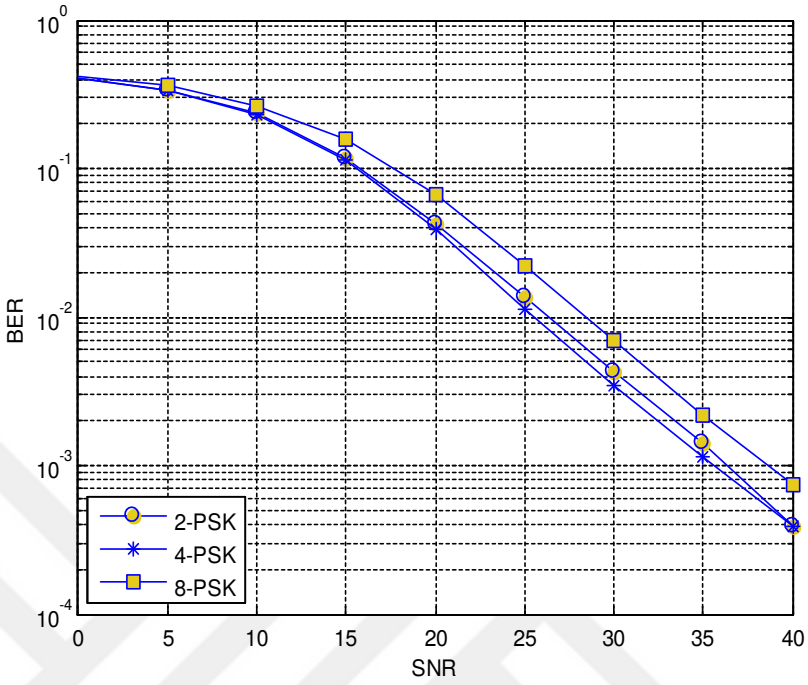

Figure 17: BER performance for different modulation types

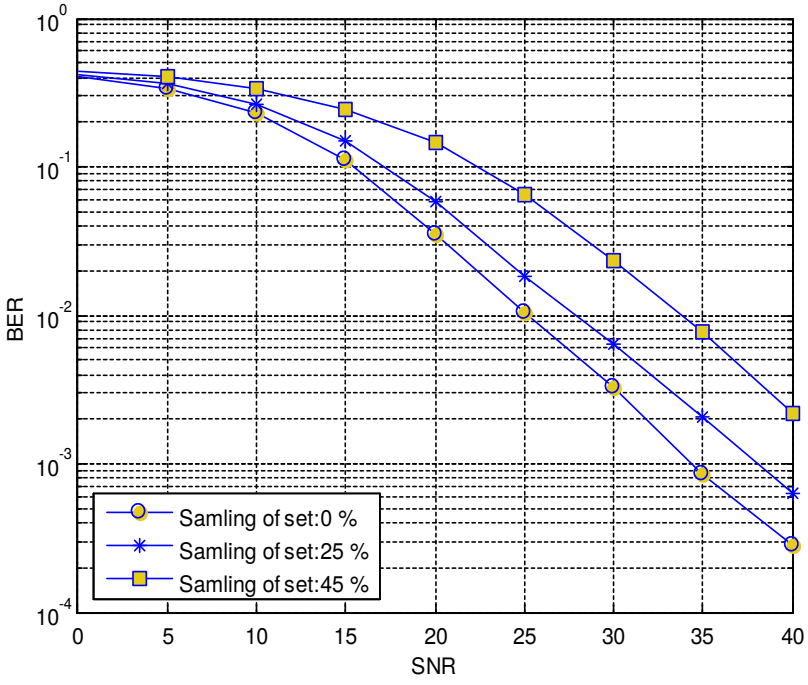

Figure 18: Evaluating the effect of sampling offset

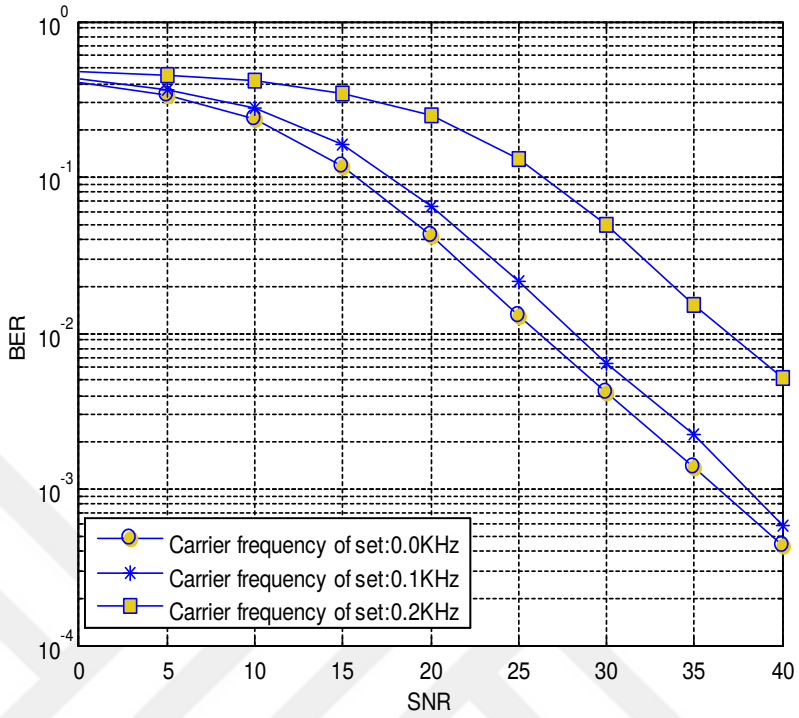

Figure 19: Evaluating the effect of frequency offset

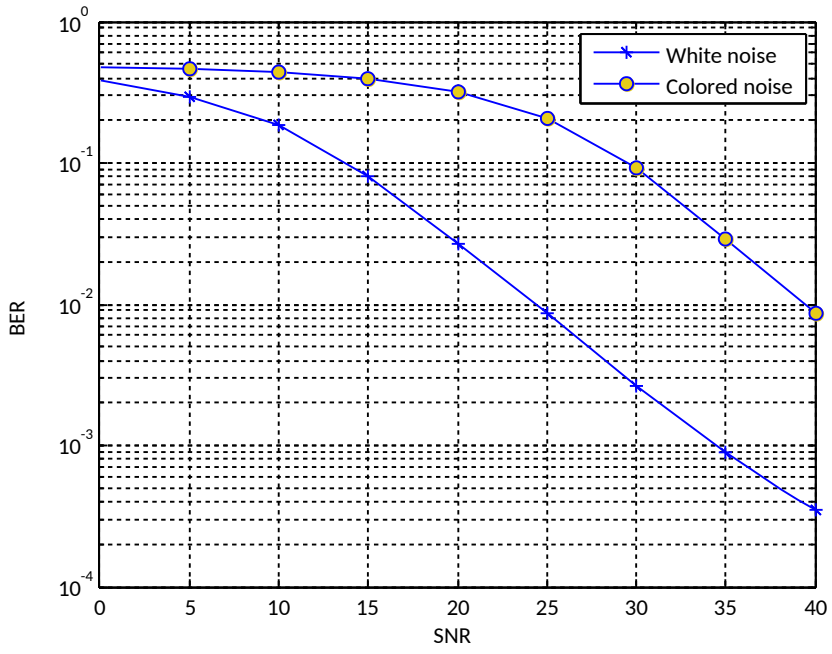

Figure 20: white versus colored Gaussian noise

CHAPTER III

USRP IMPLEMENTATION OF OFDM UWA COMMUNICATION SYSTEM

In the second chapter, we presented the Matlab implementation of OFDM-based UWA communication system and the simulation results. In this chapter we provide Labview implementation of the same system on USRP platform and present the underwater test results. We integrate our USRP system to the acoustic front-end and test the performance in the pool.

we present the implementation details of OFDM on software defined platform using Labview and National Instrument USRPs. The OFDM system under consideration is illustrated in Fig 21.

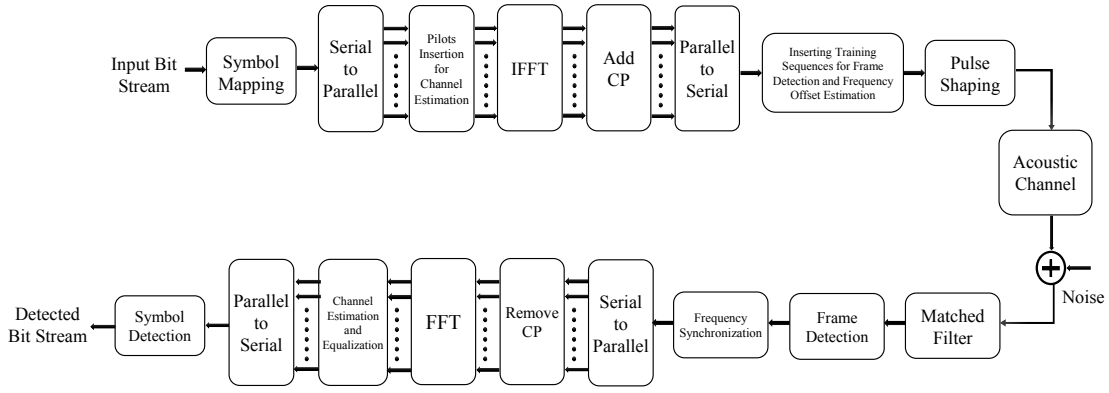

Figure 21: block diagram of the OFDM system under consideration

In the following, we go through each illustrated block and explain the implementation details of each part.

3.1 Transmitter

The overview of the transmitter side in Labview is presented in Fig 22.

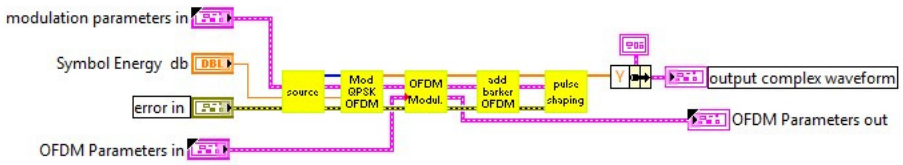

Figure 22: Transmitter blocks in Labview

3.1.1 Source and modulation blocks

The bits sequence is fed to the symbol mapping block which its output is symbols sequence $s[n]$. We consider Binary Phase Shift Keying (BPSK) and Quadrature Phase Shift Keying (QPSK). The constellation set of BPSK is given by $C = +1, -1$. The constellation set of QPSK is given by $C = 1 + j, -1 + j, -1 - j, 1 - j$.

The constellations are normalized such that

$$\frac{1}{M} \sum_{m=0}^{M-1} |s_m| = 1 \tag{7}$$

where M denotes the number of symbols in specific constellation. The normalized QPSK constellation is illustrated in Fig 23.

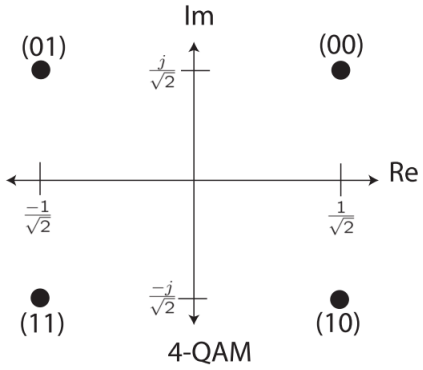

Figure 23: The normalized QPSK constellation

We implement the modulation block in Labview with "modulate.vi". Each block

in Labview is called "vi". The block diagrams of each vi file are illustrated in Figs 24,25,26.

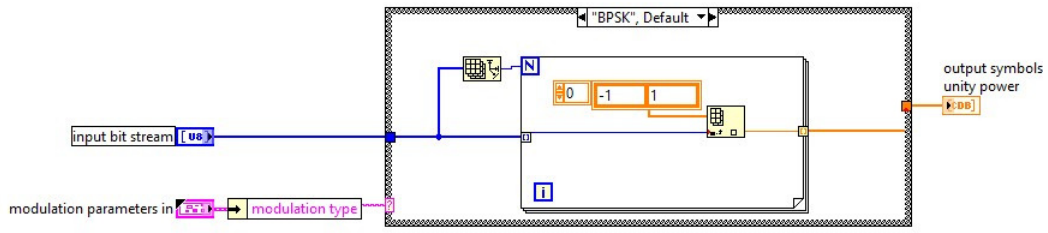

Figure 24: BPSK modulation block

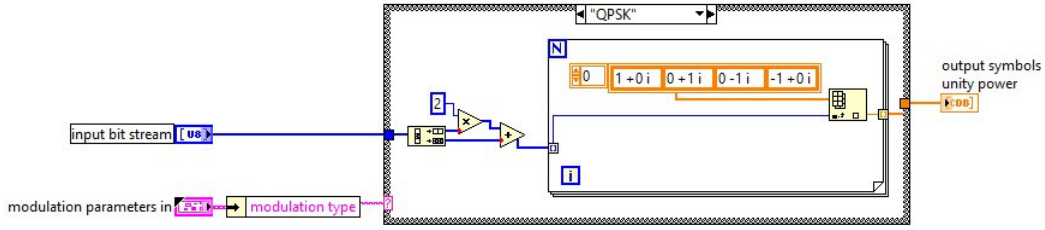

Figure 25: QPSK modulation block

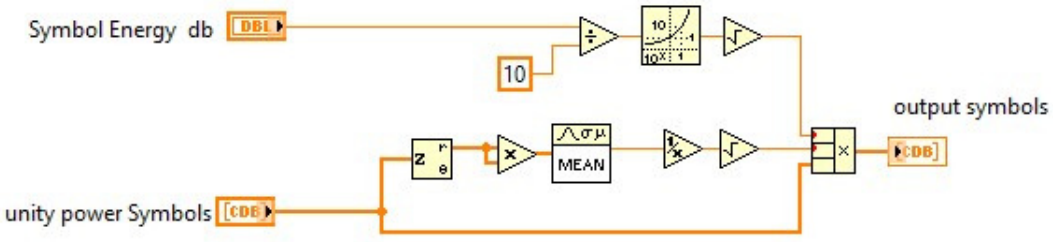

Figure 26: Symbol energy assignment

3.1.2 OFDM related transmitter blocks

We assume that one OFDM symbol consist of N symbols in frequency-domain (The number of subcarrier). Considering $\{s[n]\}_{n=0}^{N-1}$ and CP with length of L_c, the transmitter the sequence is expressed as

$$w[n] = \frac{1}{N}\sum_{n=0}^{N-1} s[m]\, e^{(j2\pi\, m(n-Lc)/N} \qquad n = 0,\ ..., N + L_c - 1 \tag{8}$$

which is passed to the transmit pulse shaping filter. The samples from $n = L_c, L_c + 1, ..., N + L_c - 1$ are the output of the inverse discrete Fourier transform (DFT) for the input symbols $\{s[n]\}_{n=0}^{N-1}$, which are implemented using the fast Fourier transform (FFT). It can be noticed that

$$w[n] = w[n + N] \qquad n = 0,\ ..., N + L_c - 1 \tag{9}$$

It can be noted that the first L_c samples of the last L_c samples of w[n] are equal which introduced as CP in previus sections. The minimum length of the CP should be equal to L_h. This will guarantee ISI free transmission for two adjacent OFDM symbols. Additionally, CP converts the linear convolution to circular convolution.

We implement the OFDM block in Labview with "OFDMt.vi". The block diagram of the of the vi is illustrated in fig 27. This vi includes some sub vis and the block diagrams of the sub vis are depicted in Figs 28-32.

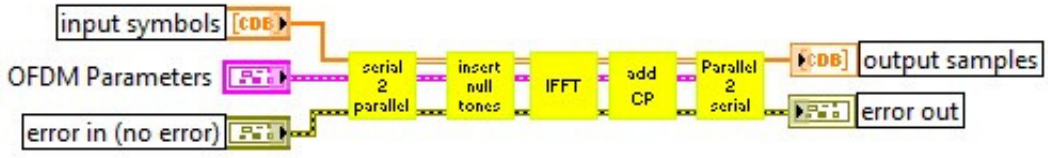

Figure 27: OFDMt.vi block diagram

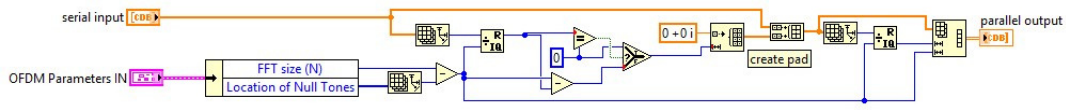

Figure 28: S2P.vi block diagram

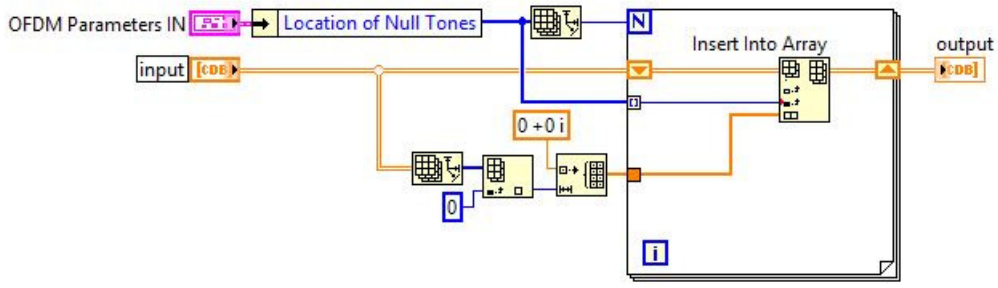

Figure 29: OFDM_insert_null_tones.vi block diagram

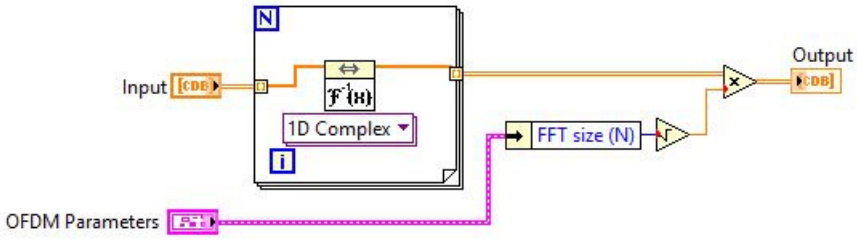

Figure 30: IFFT.vi block diagram

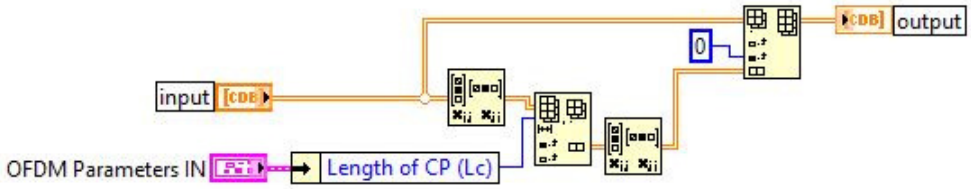

Figure 31: OFDM_add_CP.vi block diagram

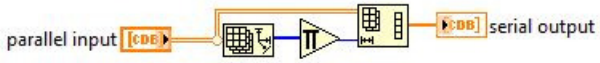

Figure 32: P2S.vi block diagram

3.1.3 Pulse shaping

Complex pulse amplitude modulated signal is created at the transmitter as following

$$x\left(t\right) \ = \sqrt{E_x} \sum_{n=-\infty}^{\infty} s\left[n\right] g_{tx}\left(t \ - nT \ \right). \tag{10}$$

The pulse shape is normalized at the transmitter in a way that $\int \left|g_{tx}\left(t\right)\right|^2 dt = 1$. At each frequency bin, the power spectrum for the transmitted signal is expressed as

$$P_x\left(f \ \right) \equiv E_x \left|G_{tx}\left(f \ \right)\right|^2 \tag{11}$$

The simplest choice of $g_{tx}\left(t\right)$ is rectangular pulse-shape but this pulse-shape is poor in spectral properties, since the Fourier transformation of a rectangular pulse shape is a sinc function, which required a large bandwidth for transmission of signal. The most common pulse shape is the raised cosine. In the frequency domain, the raised cosine pulse-shape is expressed as

$$G_{rc}\left(f\right) = \begin{cases} T, \quad 0 \leq \left|f\right| \leq \left(1-\alpha\right)/2T \\ \frac{T}{2}\left[1 + cos\frac{\pi T}{\alpha}\left(\left|f\right| - \frac{1-\alpha}{2T}\right)\right] \quad , \qquad \frac{1-\alpha}{2T} \leq \left|f\right| \leq \frac{1+\alpha}{2T} \\ 0, \qquad\qquad\qquad\qquad \left|f\right| \geq \frac{1+\alpha}{2T} \end{cases} \tag{12}$$

In time domain, it is given by

$$g_{rc} = \frac{sin\pi t/T}{\pi t/T} \frac{\cos\left(\pi\alpha t\right)}{1 - 4\alpha^2 t^2/T^2} \tag{13}$$

In (12) and (13), the parameter $0 \leq \alpha \leq 1$ is the roll off factor and expressed as the percentage excess bandwidth. At large values of α, the tails side of the pulse shape in time domain decrease quickly, while result in more excess bandwidth. Decreasing the tails of pulse shape reduces the sampling error ISI. Therefore, α can be considered as a tradeoff between excess bandwidth and resistancy to ISI. The raised cosine pulse is depicted in Fig 33.

The raised cosine pulse is not used directly at the transmitter. Since, the raised cosine represents $g(t)$ but we need $g_{tx}\left(t\right)$ at the transmitter and $g_{rx}\left(t\right)$ at the receiver.

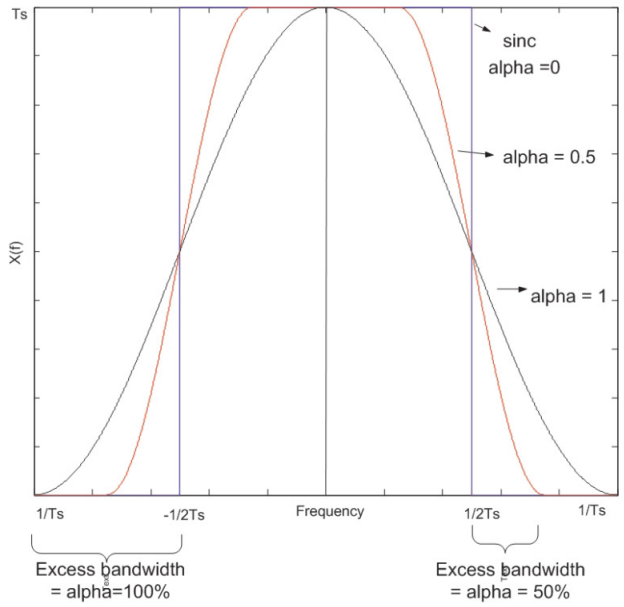

Figure 33: The raised cosine pulse

In the frequency domain this means $G(f) = G_{tx}(f) G_{rx}(f)$. We choose $g_{tx}(t)$ to be a square root of the raised cosine which is called square root raised cosine pulse shape and is written as

$$g_{sqrc}(t) = \frac{4\alpha}{\pi\sqrt{T}} \frac{\cos[(1+\alpha)\pi t/T] + \frac{\cos[(1+\alpha)\pi t/T]}{4\alpha t/T}}{1-(4\alpha t/T)^2} \tag{14}$$

Oversampling is to Sample at a rate higher than Nyquist rate. Oversampling at the analog front ends of the transceivers (DAC and ADC) result in a much simpler filters. It is also vital for efficient synchronization. Upsampling of a sequence by a factor L is eqaul to insert $L-1$ zeros between every sample of the sequence. Downsampling of a sequence by a factor M is equivalent to remove $M-1$ of every M symbols. We choose $T_x = T/L$. Choosing $c[n] = x(n_{T_x})$, we have

$$c[n] = \sum_{m=-\infty}^{\infty} s[m]\, g_{tx}(nT_x - mT) = \sum_{m=-\infty}^{\infty} s[m]\, g_{tx}[n - mL] \tag{15}$$

where $g_{tx}[n] = g_{tx}(nT_x)$. It can be noted that Eq. (9) is the output of upsampling by L, then filtering the sequence with $g_{tx}[n]$.

We implement the pulse shaping block in Labview with "pulseshaping.vi". The block diagram of the of the vi is illustrated in Fig 34.

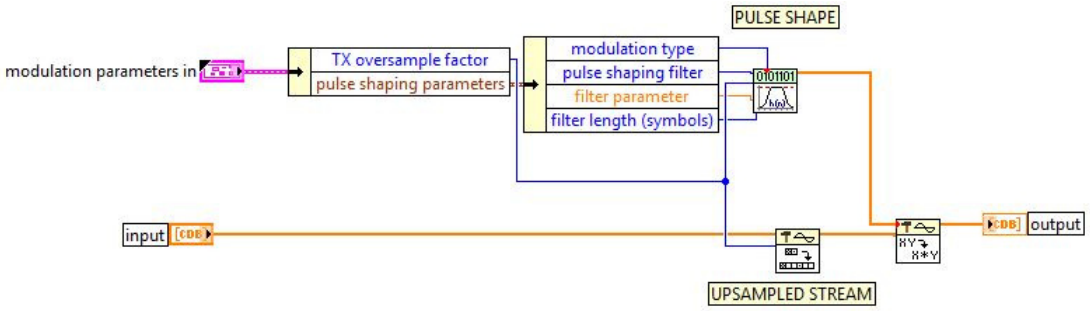

Figure 34: Pulse_shaping.vi block diagram

3.2 Receiver

The general overview of the receiver side in Labview is presented in Fig 35.

Figure 35: General overview of receiver

3.2.1 Matched filter

Let z(t) represents the complex baseband input. Choosing $T_z = T/M$ for an integer M in a way that $1/T_z$ is larger than the Nyquist rate which is called oversampling. Let $z[n] = z(nT_z)$. It is shown that

$$\begin{aligned} y[n] = \int g_{rx}(\tau)\, z(nT-\tau) &= T_z \sum_{m=-\infty}^{\infty} z[m]\, g_{rx}((nM-m)T_z) \\ &= \sum_{m=-\infty}^{\infty} z[m]\, g_{rx}[nM-m] \end{aligned} \tag{16}$$

where $g_{rx}[n] = T_z g_{rx}(nT_z)$. Eq. (16) is the result of down sampling the filtered oversampled signal $z[n]$ by $g_{rx}[n]$.

We implement the match filter block in Labview with "match_filter.vi". The block diagram of the of the vi is illustrated in Fig 36.

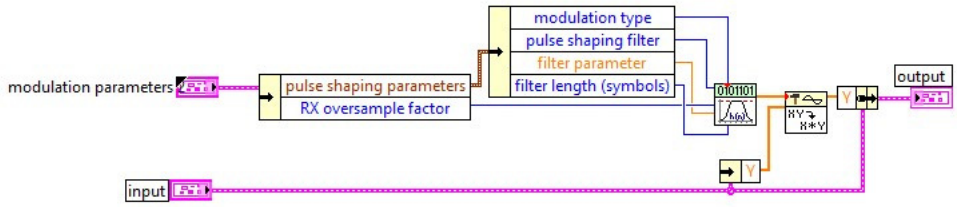

Figure 36: Match_filter.vi block diagram

3.2.2 Symbol timing recovery

The received signal is given in the form of

$$y[n] = \sqrt{E_x}\alpha e^{j\phi} s[n]\, g(\tau_d) + \sqrt{E_x}\alpha e^{j\phi} \sum_{m \neq n} s[m]\, g((n-m)T - \tau_d) + v[m] \quad (17)$$

where α, ϕ and τ_d are respectively the attenuation, phase shift and the delay. Let $g(t)$ be the convolution of $g_{tx}(t)$ and $g_{rx}(t)$. The function of output energy is defined as

$$J(\tau) = \mathrm{E}|y(nT+\tau)|^2 = E_x \sum_m |g(mT+\tau-\tau_d)|^2 + \sigma_v^2 \leq E_x \sum_m |g(0)|^2 + \sigma_v^2 \quad (18)$$

The maximum of $J(\tau)$ occurs at the time $\tau - \tau_d$ if it is being the integer multiple of symbol rate. This τ is called maximum output energy solution. if

$$r[n] = \sum_m z[m]\, g_{tx}[n-m] \quad (19)$$

denotes the matched filter output at the receiver. The output energy is computed as following

$$J[k] = E|r\ (nMT\ + k)|^2 \quad (20)$$

where k is the sample offset which is an estimate for $\hat{\tau} = kT/M$. Replacing the expectation with time average for P symbols result in the following

$$J_{approx}[k] = \frac{1}{P}\sum_{p=0}^{P-1} E|r\ (pMT\ + k)|^2 \tag{21}$$

The direct maximum output energy solution is shown by $\hat{k} = max\ J_{approx}[k]$ because in receiver only symbol synchronization is performed, evaluating $J_{approx}[k]$ for the range $k = 0, 1, ..., M-1$ is sufficient. Larger values of P generally result in a better performance.

We implement the symbol timing recovery block in Labview with "symbol_timing.vi". The corresponds block diagrams are illustrated in Figs 37 and 38.

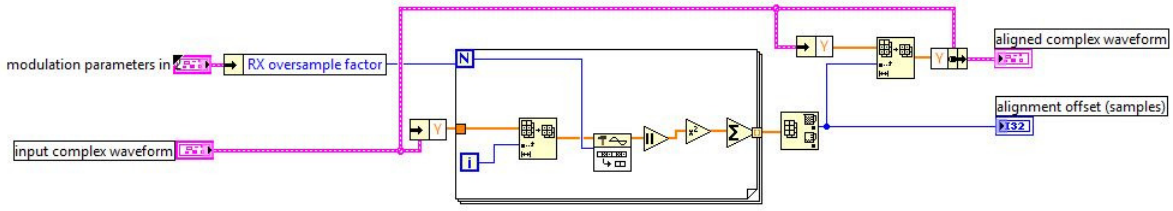

Figure 37: MaxEnergy.vi block diagram

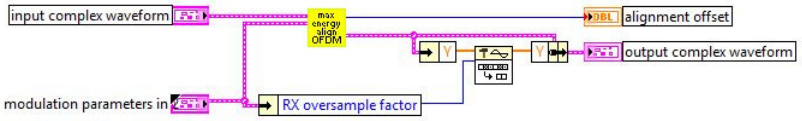

Figure 38: Symbol_timing.vi block diagram

3.2.3 Channel estimation block

In a wireless channel including underwater channels, there are multiple paths between the transceivers. In general we have:

$$z(t) = \int_{\tau} h_e(\tau)\, x(t-\tau)\, d\tau + v(t) \tag{22}$$

where $h_e(\tau)$ is the frequency selective channel at baseband. In complex pulse amplitude modulations, is distorted by channel. We propose $h(t) = \sqrt{E_x} h_e(t) * g_{tx}(t) * g_{rx}(t)$ and $h[n] = T\, h(nT)$ is the sampled channel. Then, we have

$$y[n] = \sum_m s[m]\, h[n-m] + v[n] = h[0]\, s[n] + \sum_{m \neq 0} s[m]\, h[n-m] + v[n] \tag{23}$$

There are two important issue associated with the received data in (17). First, the channel coefficients $h[l]$ create ISI. The solution is to improve the detection method by employing equalization. Second, the channel coefficients are not known at receiver. The solution estimating the channel coefficients to find the equalizer. Assuming that the composite channel $h(t)$ is FIR, equation (17) is then given by

$$y[n] = \sum_{l=0}^{L} s[m]\, h[n-l] + v[n] \tag{24}$$

Let $\{f_{n_d}[l]\}_{l=0}^{L_f}$ be an FIR equalizer. After the equalization process, we have

$$r[n] = \sum_{l=0}^{L_f} f_{n_d}[l]\, y[n-l] \approx \hat{s}[n-n_d] \tag{25}$$

where n_d is the delay of equalizer which is a designing parameter.

In our implementation, the frequency domain equalizer which is discussed in OFDM block. In AWGN, the least squares estimator is same as maximum likelihood estimation. Let $\{t[n]\}_n^{N_t} = 0$ be a known training sequence. The training sequences which is known at the receiver are inserted in the transmitted signal in a way that $s[n] = t[n]$ for $n = 0, 1, ..., N_t$. To estimate the channel coefficients we should make a of linear equations system. given

$$y[n] = \sum_{l=0}^{L} h[l]\, s[n-l] + v[n] \tag{26}$$

where $s[n] = t[n]$ for $n = 0, 1, ..., N_t$. We know $s[n]$ is unknown for $n \geq N_t$ (unknown part of signal), therefore we will find the squared error of the known data. The least

squares solution will find the estimated channel coefficients which will minimize the squared error

$$\left\{\hat{h}\left[0\right],\hat{h}\left[1\right],\ \ldots,\hat{h}\left[L\right]\right\}=\arg\min_{a[0],a[1],\ \ldots,a[L]}\sum_{n=L}^{N_t-1}y\left[n\right]-\sum_{l=0}^{L}a\left[l\right]t[n-l]^2 \tag{27}$$

The summation begins at $n = L$ which guarantees that unknown data is not considered. Our approach to this problem is to build a suitable set of linear equations. First, we form the received signal as a function of unknown with a matrix as following

$$\underbrace{\begin{bmatrix} y\left[L\right] \\ y\left[L+1\right] \\ \vdots \\ y\left[N_t-1\right] \end{bmatrix}}_{y}=\underbrace{\begin{bmatrix} t\left[L\right] & \cdots & t\left[0\right] \\ \vdots & \ddots & \vdots \\ t\left[N_t-1\right] & \cdots & t\left[N_t-1-L\right] \end{bmatrix}}_{T}\underbrace{\begin{bmatrix} a\left[0\right] \\ a\left[1\right] \\ \vdots \\ a\left[L\right] \end{bmatrix}}_{a} \tag{28}$$

where we refer to T as the training matrix. If T is square or tall and full rank, then $T * T$ is an invertible square matrix. The tall assumption (square with equality) requires that

$$N_t-L\geq L+1 \tag{29}$$

or, equivalently

$$N_t\geq 2L+1 \tag{30}$$

Generally, N_t much larger than $L+1$ (the length of the channel) results in better performance.

We implement the channel estimation block in Labview with "channel_estimate.vi". The corresponding block diagrams are illustrated in Figs 39 and 40.

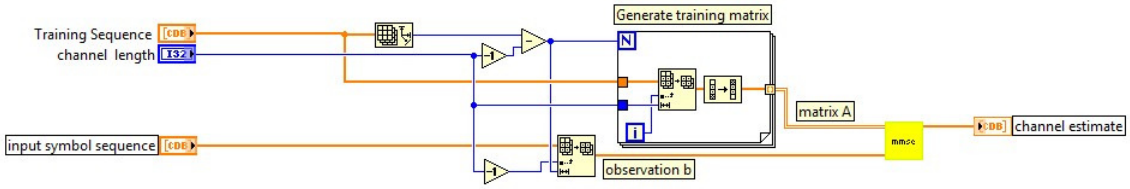

Figure 39: Channel_estimate.vi block diagram

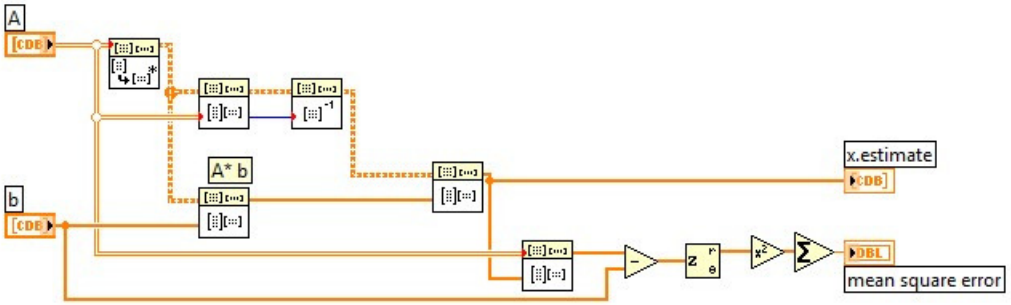

Figure 40: Least_square.vi block diagram

3.2.4 Frame synchronization and frequency offset correction

The purpose of frame synchronization is to determining the beginning of the frame. We consider an approach regarding correlation properties of the training signal. we neglect the effect of carrier frequency to develop frame synchronization in this section. Assuming a flat channel in which symbol synchronization already has been done then we have

$$y\left[n\right] = \ hs\left[n-d\right] + \ v\left[n\right] \tag{31}$$

After matched filtering and down sample, h and d are unknown channel coefficients and unknown frame-offset. Assume that frames include a training signal length N_t and data symbols of length PN_t and $\{t\left[n\right]\}_{n=0}^{N_t}$ is the training sequence known at the receiver. Considering good correlation properties of the training sequence, the

received signal is correlated with the training data to calculate

$$R[n] = \left| \sum_{k=0}^{N_t-1} t*[k]\, y[n+k] \right|^2 \tag{32}$$

and find the frame-offset as following

$$\hat{d} = \max_n R[n] \tag{33}$$

This correlation in Eq. (26) leads to two terms

$$R[n] = \left| \sum_{k=0}^{N_t-1} t*[k]\, hs[n-d] + \sum_{k=0}^{N_t-1} t*[k]\, v[n] \right|^2 \tag{34}$$

Since we have zero mean, the second part is approximately zero when the training sequence is large. This result in

$$R[n] = \left| \sum_{k=0}^{N_t-1} t*[k]\, hs[n+k-d] \right|^2 = |h|^2 \left| \sum_{k=0}^{N_t-1} t*[k]\, s[n-d] \right|^2 \tag{35}$$

Since the data is different from the training sequence, the correlation maximum point occurs at the point of the training signal, considering that the observation includes the inserted training data.

In practice, the carrier frequency of up conversion at the transmitter is not matching the carrier frequency at the receiver which results in a carrier frequency offset. The offset leads to rotatation the received signal by $exp(j2\pi f_o t)$ where f_o is the difference between the frequency at receiver and transmitter. The more the offset, the more the received signal rotates. This offset affects most of processes at the receiver including synchronization, channel estimate, and equalizing. Assuming we have small carrier offset , sampling can be employed and the discrete-time signal at the receiver after matched filter and down sample is given by

$$y[n] = e^{j2\pi n\varepsilon} \sum_{l=0}^{L} h[l]\, s[n-l] + \ v[n] \tag{36}$$

where $\varepsilon = f_o T$. The idea of carrier frequency synchronization is to estimate ε. Having an estimate $\hat{\varepsilon}$, removing of the offset to perform

$$\hat{y}\left[n\right] = e^{-j2\pi\varepsilon n} y\left[n\right]. \tag{37}$$

An algorithm proposed by Moose [7] is employed to estimate the carrier frequency offset. It is a self-referenced synchronization method. Assume pulse-amplitude modulation with the repetition of two training sequences followed by the data. If the training sequence begins at $n = 0$. We have

$$s\left[n\right] = \ s\left[n + N_t\right] = \ t\left[n\right] \tag{38}$$

for $n = 0, 1, ..., N_{t-1}$. It can be noted that symbols $s[n]$ for $n < 0$ and $n \ \geq \ N_t$ are unknown. For $L \leq n \leq N_t - 1$, we have

$$\begin{aligned} y\left[n\right] &= e^{j2\pi\varepsilon n} \sum_{l=0}^{L} h\left[l\right] s\left[n-l\right] + \ v\left[n\right] \\ y\left[n+N_t\right] &= e^{j2\pi\varepsilon(n+N_t)} \sum_{l=0}^{L} h\left[l\right] s\left[n-l\right] + \ v\left[n\right] \end{aligned} \tag{39}$$

Using the fact that $s[n + N_t] = s[n] = t[n]$ for $n = 0, 1, ..., N_t - 1$, we can write

$$y\left[n+N_t\right] = \ e^{j2\pi\varepsilon N_t} e^{j2\pi\varepsilon n} \sum_{l=0}^{L} h\left[l\right] t\left[n-l\right] + \ v\left[n+N_t\right] y[n+N_t] \approx \ e^{j2\pi\varepsilon N t} y\left[n\right] \tag{40}$$

One approach is the formulation and solving a least-squares problem. Since ε is in the exponent term, we modify least squares problem. Assume the squared error as

$$J\left(a\right) \ = \sum_{l=L}^{N_t-1} y\left[l \ + N_t\right] - \ a y[l]^2 \tag{41}$$

where the coefficient a can be estimated through

$$\hat{a} = \frac{\sum_{l=L}^{N_t-1} y\left[l \ + N_t\right] y^*\left[l\right]}{\sum_{l=L}^{N_t-1} \left|y\left[l\right]\right|^2} \tag{42}$$

Since only the phase of a is of interest, there is no need to compute the denominator. A basic estimation of the frequency offset is achieved as

$$\hat{\varepsilon} = \frac{phase \sum_{l=L}^{N_t-1} y\left[l+N_t\right] y^*\left[l\right]}{2\pi N_t} \tag{43}$$

$$\widehat{f_e} = \frac{phase \sum_{l=L}^{N_t-1} y\left[l+N_t\right] y^*\left[l\right]}{2\pi T N_t} \tag{44}$$

Larger N_t improves the estimation since it imposes more noise averaging but decrease the offset correction range.

We implement the frequency offset correction and frame synchronization block in Labview with "freq_estimate.vi". The corresponding block diagrams of the of the vis are illustrated in Figs 41-44.

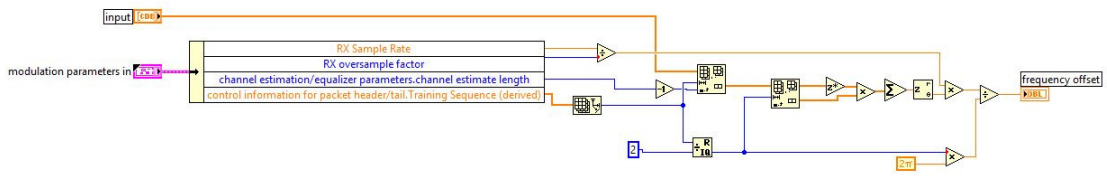

Figure 41: Freq_estimate.vi block diagram

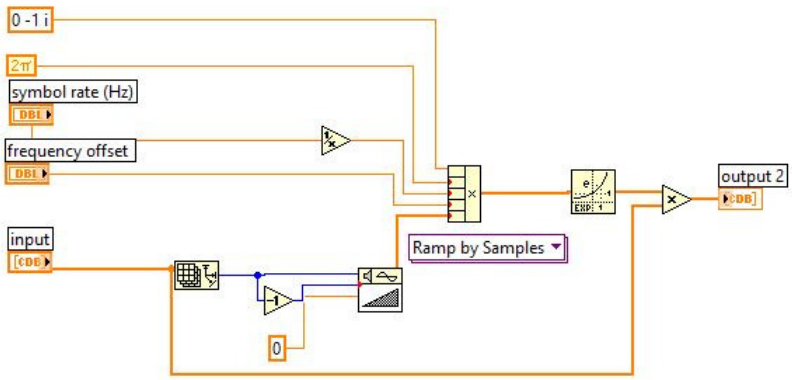

Figure 42: Freq_correction.vi block diagram

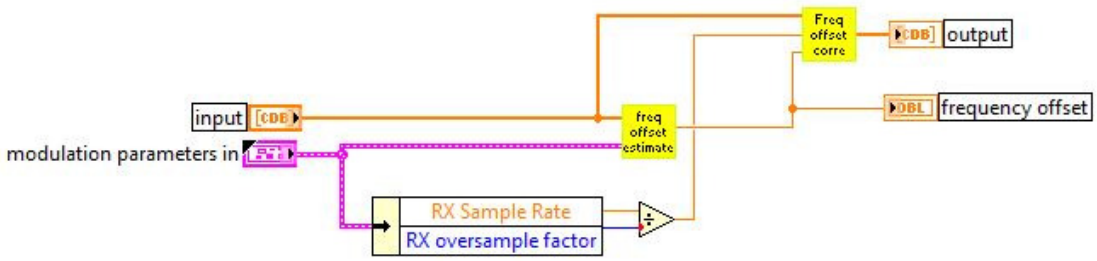

Figure 43: Moose.vi block diagram

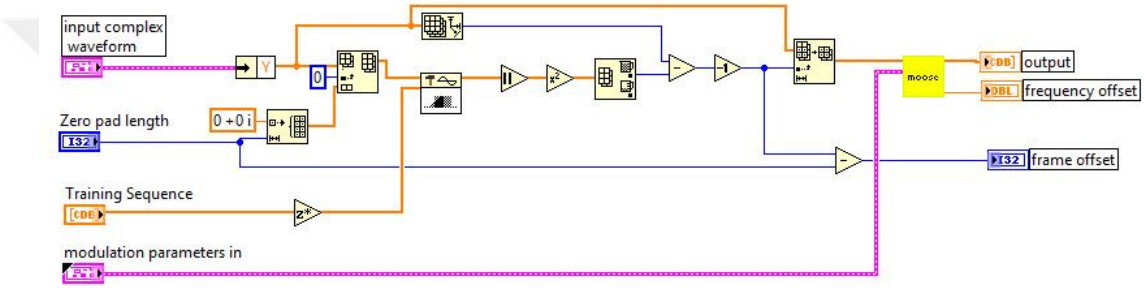

Figure 44: Frame_sync.vi block diagram

3.2.5 OFDM related receiver blocks

After matched filter, symbol timing, frame synchronization, down sample, frequency and frame synchronization the received signal can be expressed as

$$y\left[n\right] = \sum_{l=0}^{L} h\left[l\right] w\left[n-l\right] + \ v\left[n\right] \tag{45}$$

The receiver eliminates the first L_c samples to form for $n = 0, 1, ..., N-1$ (neglecting noise) $\bar{y}\left[n\right] = \ y\left[n \ + \ L_c\right]$. With some mathematical changes, it can be seen that

$$\begin{aligned}
\bar{y}[n] &= \sum_{l=0}^{L} h[l]\, w[n+L_c-l] \;\; n \;=\; 0,\; ..., N-1 \\
&= \; \tfrac{1}{N} \sum_{l=0}^{L} h[l] \sum_{m=0}^{N-1} s[m]\, e^{j2\pi \frac{m(n+L_c-L_c-l)}{N}} \\
&= \; \tfrac{1}{N} \sum_{l=0}^{L} h[l] \sum_{m=0}^{N-1} s[m]\, e^{j2\pi \frac{mn}{N}} s[m]\, e^{-j2\pi \frac{ml}{N}} \\
&= \; \tfrac{1}{N} \sum_{m=0}^{N-1} \left(\sum_{l=0}^{L} h[l]\, e^{-j2\pi \frac{ml}{N}} \right) s[m]\, e^{j2\pi \frac{mn}{N}}
\end{aligned} \tag{46}$$

Then the receiver takes the DFT or FFT of samples to produce

$$\bar{Y}[k] = DFT[\bar{y}[n]] = H[k]\, s[k] + V[k] \tag{47}$$

where

$$H[k] = \sum_{l=0}^{L} h[l]\, e^{j2\pi \frac{kl}{N}} \tag{48}$$

which is the DFT of the zero padding channel. The frequency domain interpretation of OFDM achieved from Eq. (45). The information on the k^{th} discrete-time sinusoid faces the channel response represented by $H[k]$. Equalization requires to divide $\bar{Y}[k]$ by $H[k]$. This is referred as the frequency domain equalizer (FEQ).

The cyclic prefix length L_c should be at least the order of the channel response L_h. The guard interval is a form of overhead that result in lower effective data. In practical systems the guard interval is determined based on maximum delay spread. By increasing the bandwidth, L_c must increase to compensate and larger N results in the smaller the subcarrier spacing. The subcarrier spacing shows the sensitivity to Doppler and residual carrier frequency offset.

We implement the receiver OFDM block in Labview with OFDMr.vi. The block diagram of the of the vi is illustrated in Fig 45. This vi includes some sub vis. The block diagrams of the sub vis are depicted in Figs 46-52.

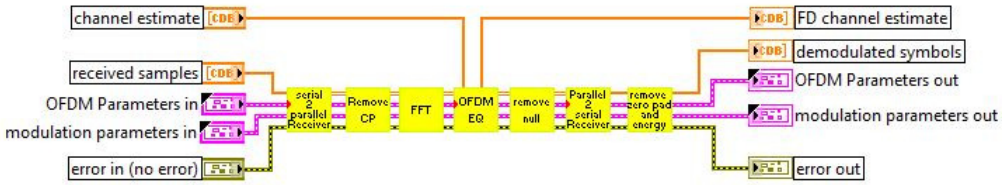

Figure 45: OFDMr.vi block diagram

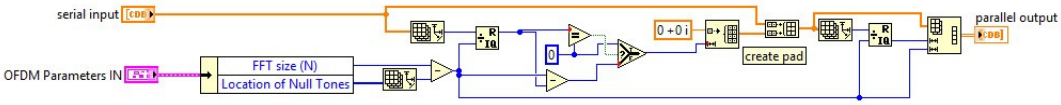

Figure 46: S2P.vi block diagram

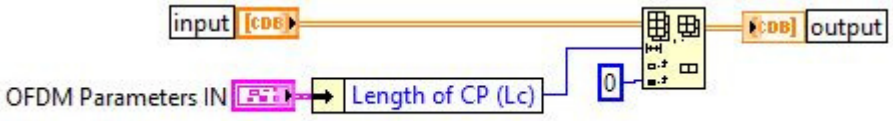

Figure 47: OFDM_remove_CP.vi block diagram

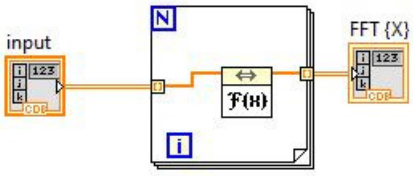

Figure 48: FFT.vi block diagram

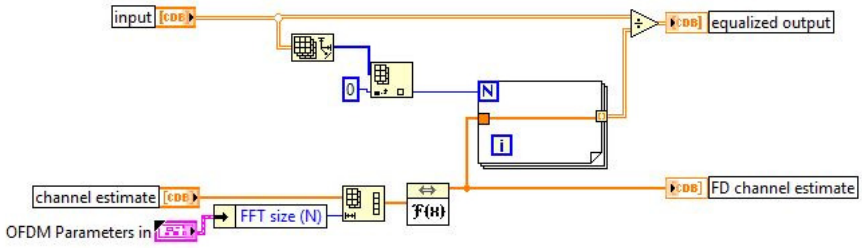

Figure 49: OFDM_FEQ.vi block diagram

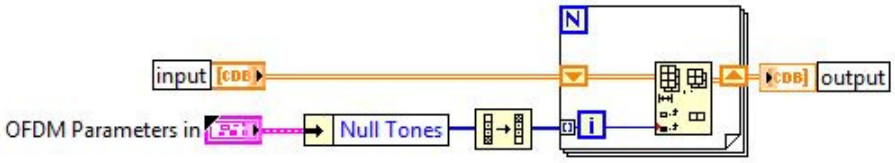

Figure 50: OFDM_remove_null_tones.vi block diagram

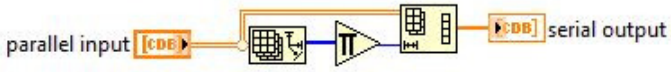

Figure 51: P2S.vi block diagram

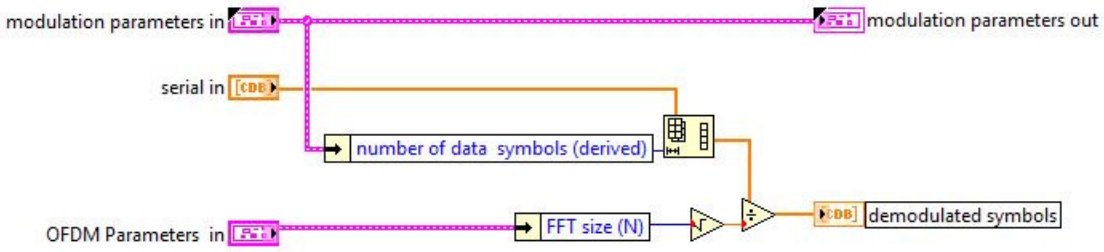

Figure 52: OFDM_demodulator.vi block diagram

3.2.6 Detection blocks

The optimal receiver design includes matched filter, sampler, and detection. The received signal $z(t)$, which is bandlimited, is sampled at the rate of $1/T_z$. The sampling rate should follow the Nyquist. We suppose that $T_z = T/M$ where M is the integer multiple of oversampling. The received signal is filtered by $g_r x[n] = g_r x(nT_z)$ where $g_r x(t) = g_t x(-t)$ is the matched filter. After the digital filtering, the signal is downsampled by M producing the symbol-rate sampled signal which given by $y[n]$. The digital filtering is performed in a way that $y[n]$ is the equivalent to $y(t) = \int_t g_{rx}(\tau) z(t - \tau) d\tau$ sampled at T . A model for the received signal is

$$y\left[n\right] = \sqrt{E_x}s\left[n\right] + v\left[n\right], \tag{49}$$

where $v[n]$ is i.i.d. complex Gaussian noise with $\mathcal{N}_c\left(0, \sigma_v^2\right)$ where $\sigma_v^2 = N_0$. A symbol detection is an algorithm that given the observation $y[n]$ produces the best $\hat{s}\left[n\right] \in \mathcal{C}$ according to the specific criterion. We consider the maximum likelihood (ML) criterion which try to solve

$$s\left[n\right] = \arg\max_{s\in\mathcal{C}} f_{y|s}\left(y\left[n\right]|s\left[n\right] = s\right), \tag{50}$$

where $f_{y|s}\left(\cdot\right)$ is the conditional distribution of $y[n]$ where $s[n]$ is given and known as the likelihood function. For AWGN, it is given by

$$\hat{s}\left[n\right] = \arg\min_{s\in\mathcal{C}} \left|y\left[n\right] - \sqrt{E_x}s\left[n\right]\right| \tag{51}$$

Given $y[n]$, it determines the transmitted symbol $s \in \mathcal{C}$, scaled by $\sqrt{E_x}$, which is closest to $y[n]$ considering the Euclidean distance in the error term $y\left[n\right] - \sqrt{E_x}s$.

We implement the symbol detection in Labview with "demodulator.vi". The corresponding block diagrams of the of the vis are illustrated in Figs 53-54.

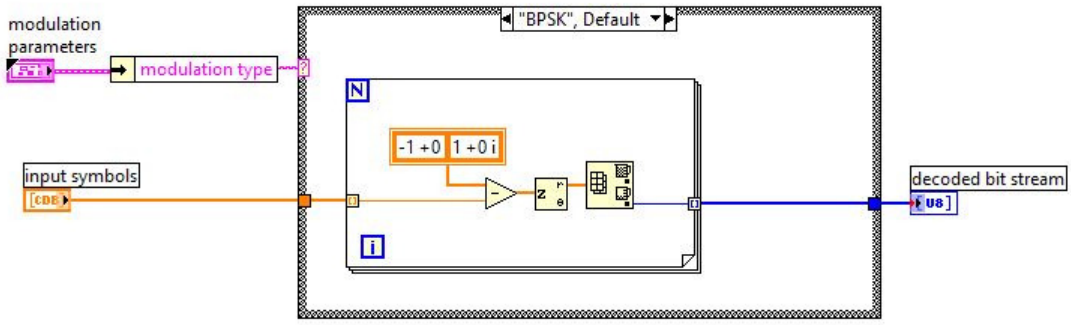

Figure 53: BPSK_demodulator.vi block diagram

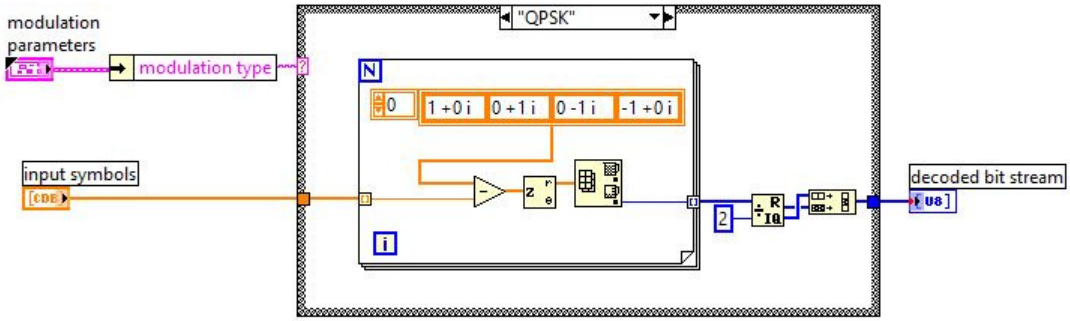

Figure 54: QPSK_demodulator.vi block diagram

3.3 Experimental results

Fig 55 shows the general block diagram of our experimental setup. Each block is explained with details in the following:

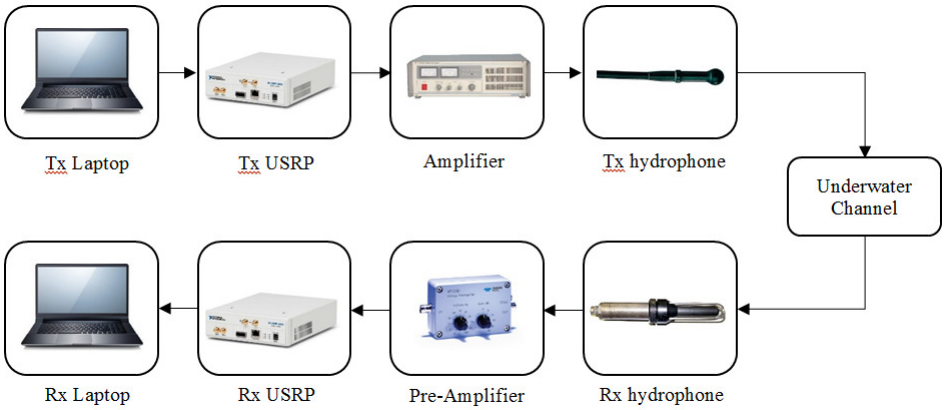

Figure 55: Block diagram of experimental set-up

Tx Laptop: The transmitter side laptop generates OFDM symbols using LabVIEW. LabVIEW Communication Toolbox is used in order to connect software environment to USRP hardware. The data is transmitted with Ethernet cable from Laptop to USRP.

Tx USRP: NI USRP 2930 is used as an interface that allows the generation

of the analog signal at the desired sampling rate. This USRP is customized and equipped with Baseband card with output sampling rate up to 5 MHz to suit for acoustic communication.

Amplifier: The signal transmitted by the NI USRP is further amplified by YE5873A Power amplifier to adjust the signal power for the input of acoustic hydrophone.

Tx hydrophone: The hydrophone is omni-directional which is built and provided at Suasis company. It is suitable for transmitting range of 20KH to 40KH. 30KH is chosen as the carrier frequency for our tests.

Rx hydrophone: The hydrophone which is built and provided at Suasis company has been chosen for receiving the acoustic OFDM signal.

Pre-Amplifier: Once the signal is received by hydrophone, the Reson VP1000 preamplifier amplifies and filters the received signal.

Rx USRP: NI USRP2930 is used and equipped with baseband card with input sampling rate up to 5 MHz to suit for acoustic receiver. The received analog signal at the USRP is sampled and digitized to produce desired digital signal and transmit it to laptop through Ethernet cable for further processes.

Rx Laptop: The receiver side laptop receives the digital signal. The received signal is processed in LabVIEW with the aid of Communication Toolbox to detect the transmitted data.

The geometry of the experiment is given in Fig 56. The transmitter and receiver are submerged in the pool at a depth of 2 meters. The distance between transmitter and receiver is varied between 0.5 to 2 meters.

In Fig 57 to 59, the photos of Suasis indoor pool where the experiments took place and experimental set-up are shown.

Experiments are performed to test the performance of the designed system. The system parameters are summarized in Fig 60. In this experiment, text with length

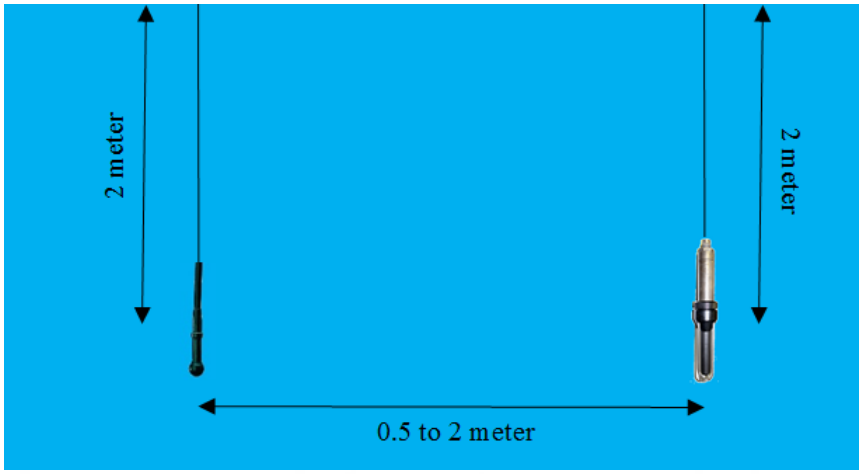

Figure 56: Geometry of the experimental set-up

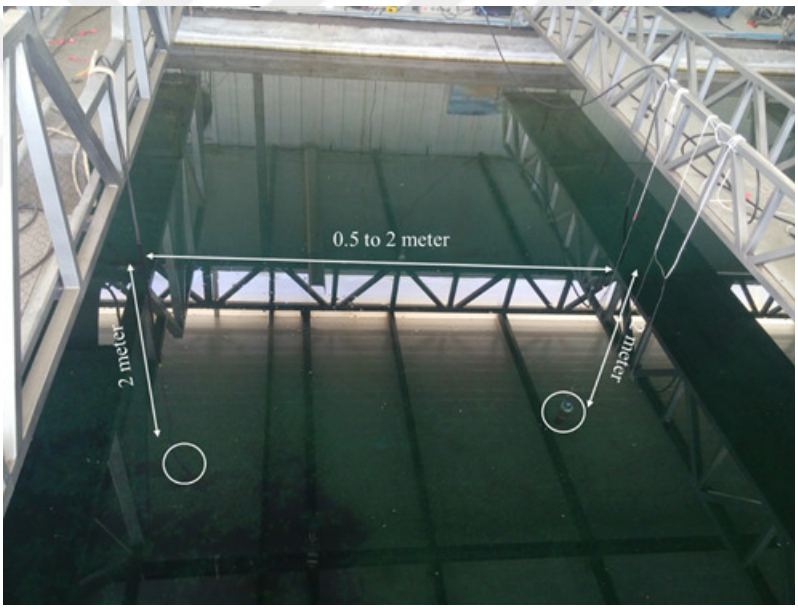

Figure 57: Indoor pool facility

up to 4000 characters is transmitted. The transmitted text is "this is underwater acoustic communication test which is done using USRP and acoustic facility".

In Figs 61 and 62, time domain representation of transmitted and received signals are shown respectively. These signals are shown in both LabVIEW environment and oscilloscope.

In Fig 63, the constellation diagram is shown at the transmitter side (Fig 63,

Figure 58: Experimental set-up implementation

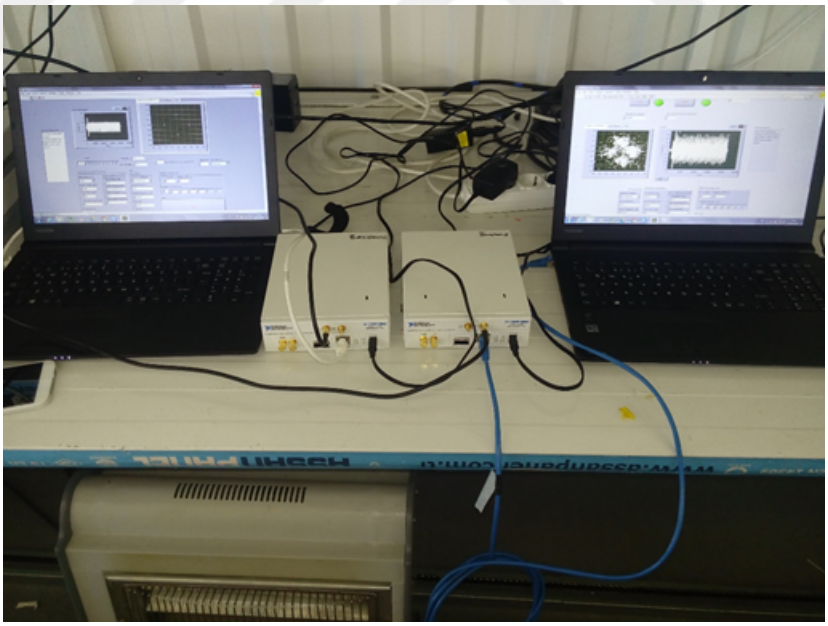

Figure 59: USRP set-up

a) and at the receiver side (Fig 63, b to e). In b to d, it can be observed that as the power decreases (lower SNR) the constellation gets closer.Therefore the detection performance gets poor and results in wrong detection of the text file. Underwater

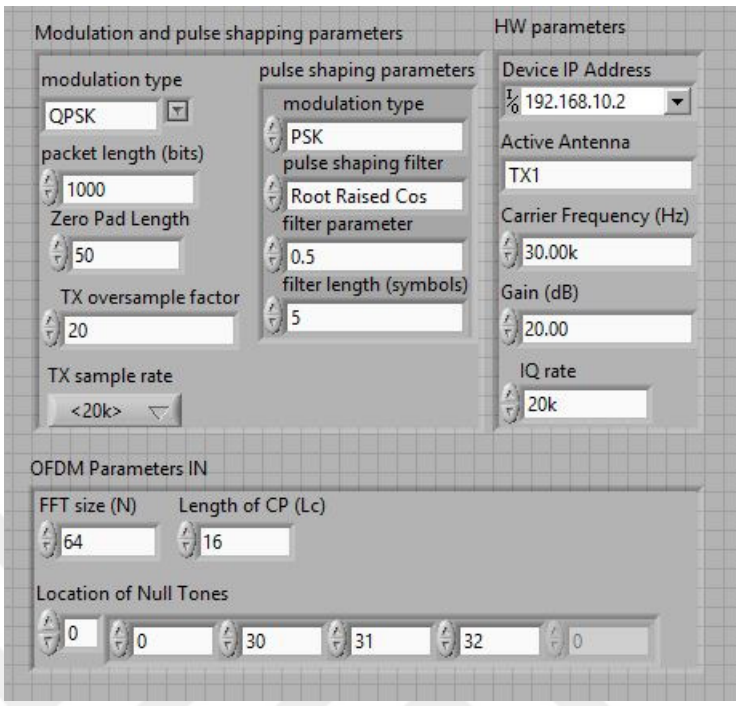

Figure 60: System parameters used in the experimental tests

environment is a noisy environment and correct detection of the text is not possible even in highest transmit power which can be provided by our practical implementation. Therefore we have implemented repetition code to have the correct detection of the transmitted text (Fig 63, e).

In Fig 64, the eye diagram is shown at the transmitter side (Fig 64, a) and at the receiver side (Fig 64, b to e). In b to d, it can be observed that as the power decreases (lower SNR) the eye gets closer. Therefore the detection performance gets poor and results in wrong detection of the text file. In e, eye diagram is shown for repetition code to have the correct detection of the transmitted text.

In Figs 65 and 66, BER is plotted versus transmit SNR and receive SNR power respectively. It could be noticed that as the SNR increases, BER decreases.

In Fig 67, BER is plotted versus packet index for different distances at a specific transmit power (6 dB). It shows that as the distance increases, BER increases.

In Fig 68, BER is plotted versus distance at a specific transmit power (6 dB).

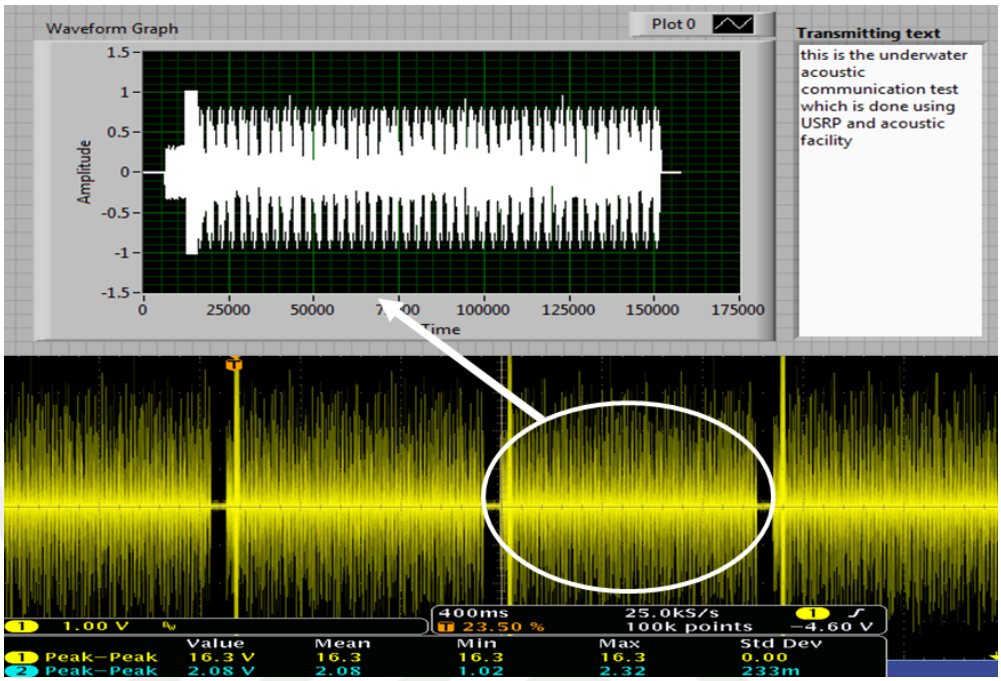

Figure 61: Transmitted text signal in time domain

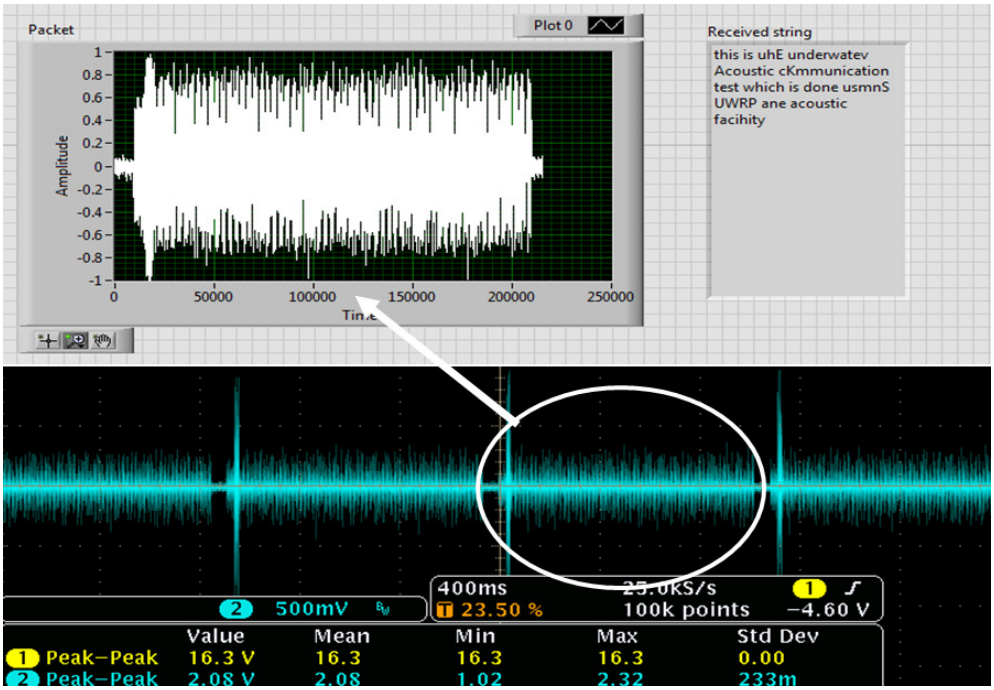

Figure 62: Received text signal in time domain

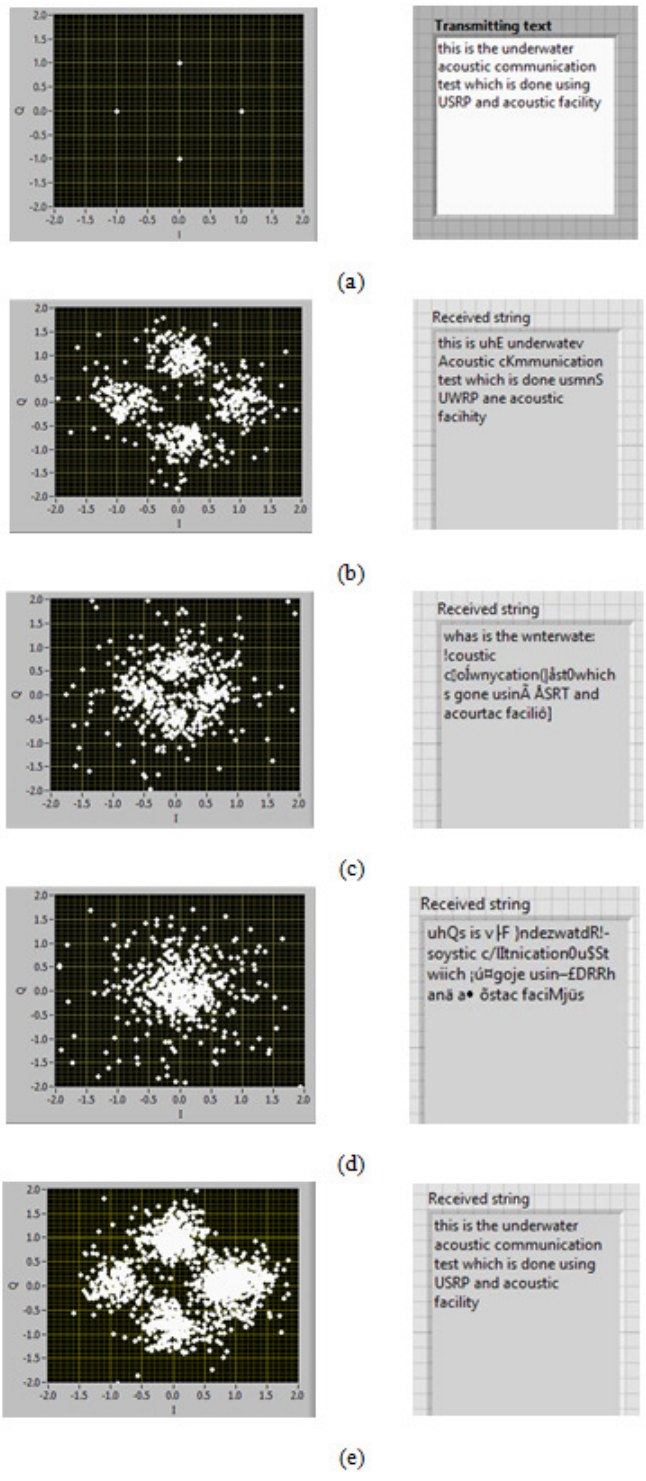

Figure 63: Constellation diagram

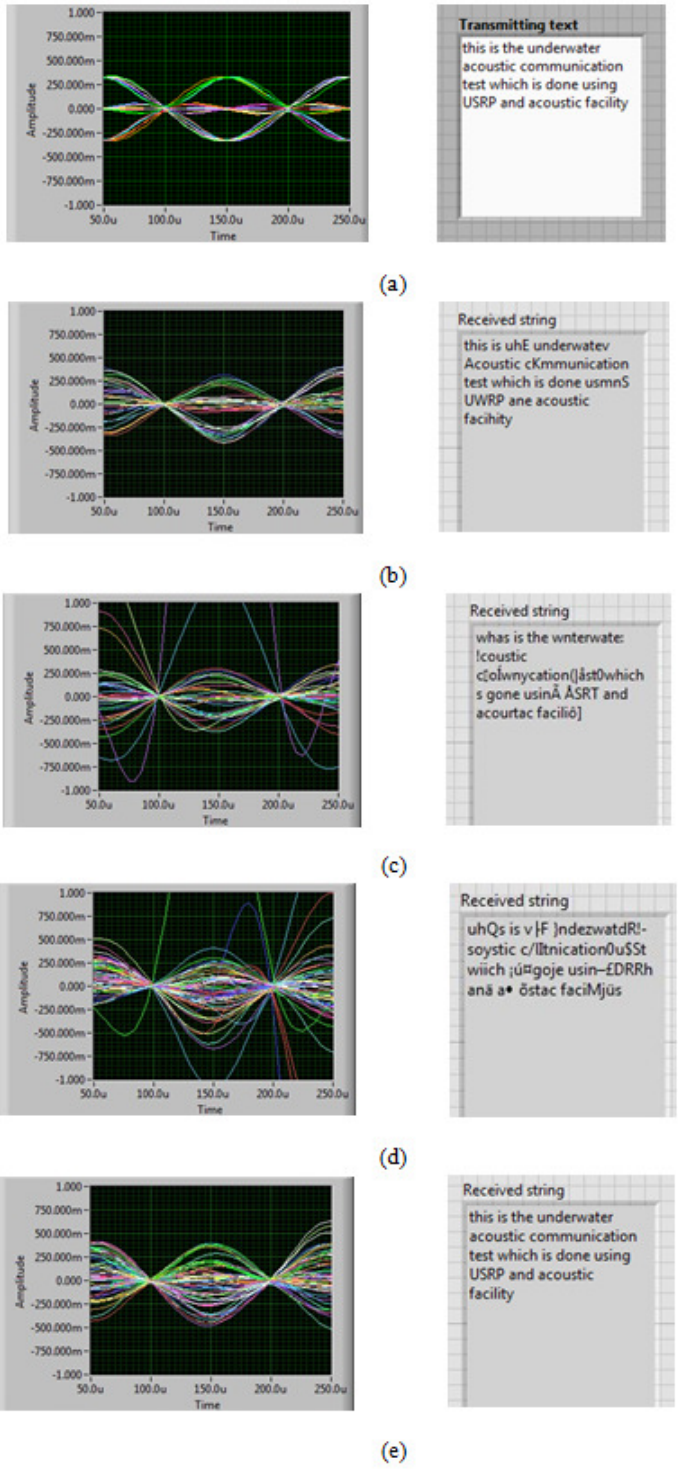

Figure 64: Eye diagram

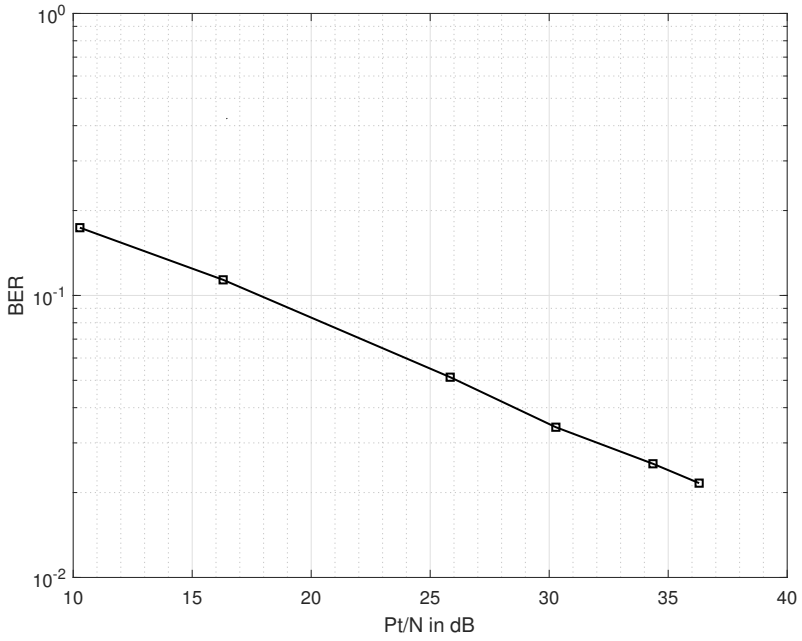

Figure 65: BER versus transmit SNR

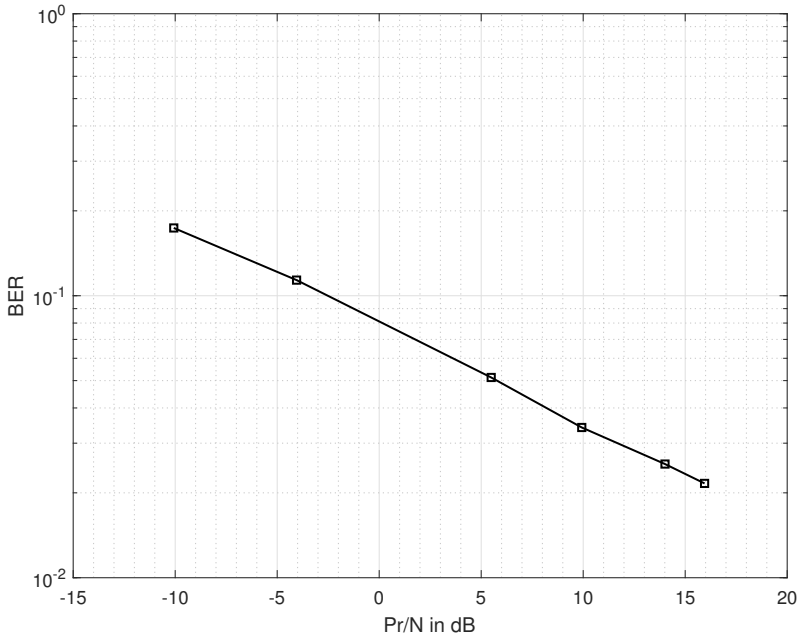

Figure 66: BER versus received SNR

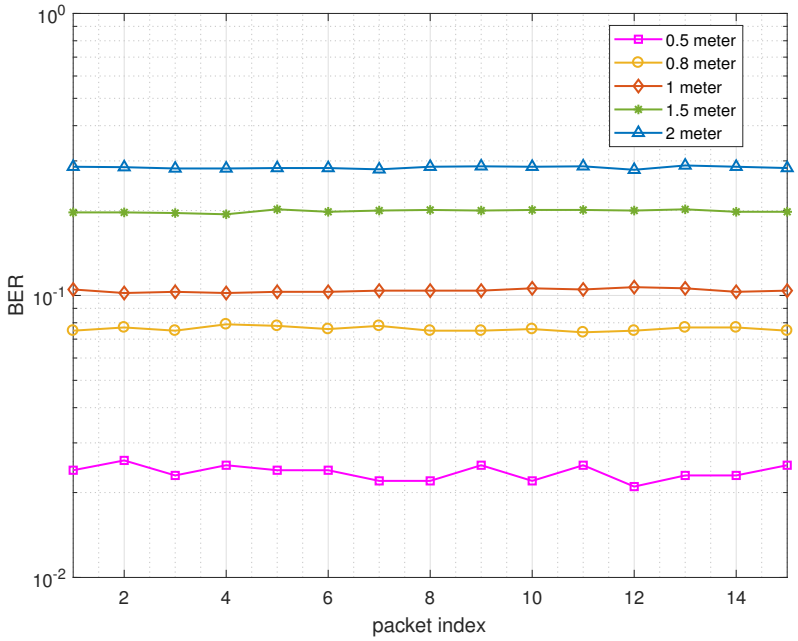

Figure 67: BER versus packet index

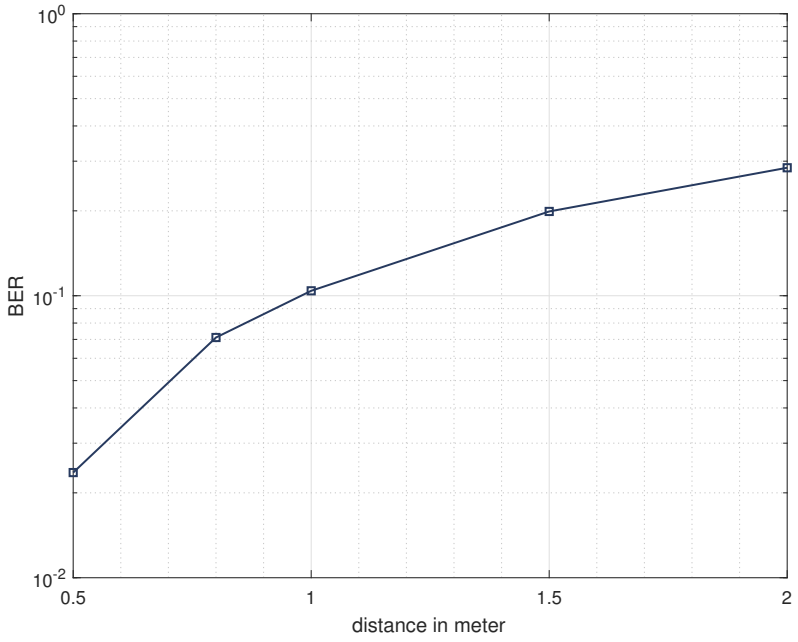

Figure 68: BER versus distance

CHAPTER IV

ADAPTIVE OFDM UWA SYSTEM

Although adaptive transmission techniques have been widely investigated for radio frequency channels, see e.g., [35, 36, 37], the literature on adaptive UWA communication systems is rather sparse. In ., [38], a UWA system with adaptive power control is considered, where the transmitter adjusts its power so that the received power remains at a specified level. Two spectrally efficient adaptive schemes are proposed in [39] to allocate bits and power across the OFDM subcarriers. In [40], adaptive modulation and coding for UWA OFDM is proposed in which instantaneous signal-to-noise ratio (SNR) is used for mode switching. In [41], the throughput is maximized by choosing best modulation while achieving a fixed bit error rate (BER).

In our work, we consider an adaptive SISO OFDM scheme where modulation size/type and transmit power are chosen as adaptive parameters. The aim is to maximize throughput by assigning different modulation size/type and transmit power to each subcarrier while maintain the average BER at a fixed value.

4.1 System model

Fig 69 depicts the block diagram of adaptive system under consideration. We consider an OFDM system with K subcarriers where the n-th block of the information bearing symbol is denoted as $S_{k,n}$. The adopted modulations are BPSK, QPSK, 8-QAM and 16-QAM. For the k-th subcarrier of the n-th block, the modulation level is denoted as $M_{k,n} \in \{2,\ 4,\ 8,\ 16\}$. The channel is considered to be fixed at least over for the period of one OFDM block. It is a sparse channel with Rayleigh distribution and decaying power profile (see chapter 2).

After removal of the CP, the received signal for the k-th subcarrier of the n-th

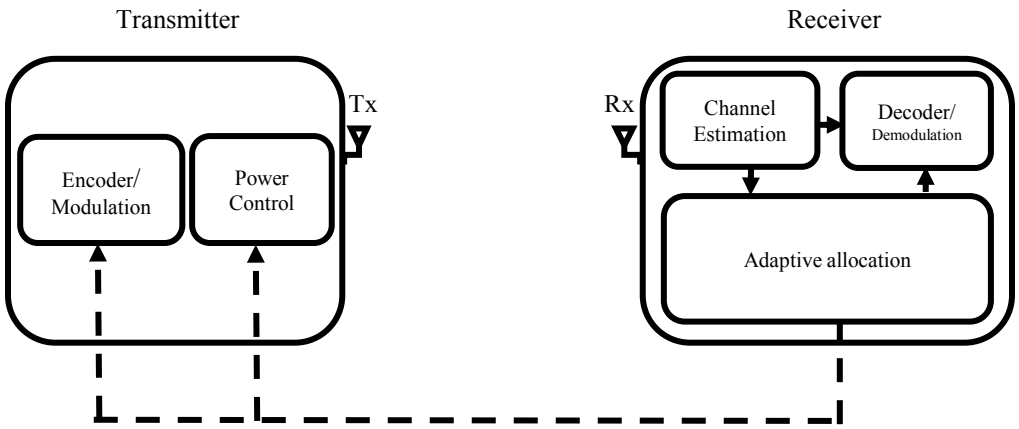

Figure 69: Adaptive system model

OFDM block can be expressed as

$$Y_{k,n} = H_{k,n}\sqrt{G_{k,n}}S_{k,n} + W_{k,n} \tag{52}$$

where $Y_{k,n}$, $H_{k,n}$, $G_{k,n}$, and $W_{k,n}$ are, respectively, the frequency-domain received signal, the gain of channel , the transmission power, and complex white Gaussian noise with zero mean and unit variance of σ_W^2 (AWGN). Assuming perfect channel estimation at the receiver, we compute the adaptive metrics (modulation type/size and power level of each subcarrier) and feed them back to transmitter.

We consider three different adaptive schemes. In the first and the second scheme, bit allocation (through the choice of proper modulation type/size) is made adaptively to each subcarrier and the power is equally distributed among subcarriers. The third scheme allocates both modulation and power adaptively based on the CSI at the subcarrier.

Adaptive Algorithm 1: The algorithm design is formulated as a constrained

optimization problem as

$$\begin{aligned} &\max_{M_{0,n},\ldots,M_{K-1,n}} \sum_{k=0}^{K-1} \log_2 M_{k,n} \\ &subject\,to: \ \tfrac{1}{K}\sum_{k=0}^{K-1} P_{e,k} \le P_b \\ &G_{k,n} = \tfrac{1}{K} G_n \end{aligned} \tag{53}$$

where G_n is the overall average power allocated to the n-th OFDM block, $P_{e,k}$ is the average BER for the k-th sub-carrier, and P_b is the target BER.

Under the assumption that the current channel gain $H_{k,n}$ is perfectly known, bit error rate of the k-th sub-carrier for MQAM modulation is approximated by [35]

$$P_{e,k}(H_{k,n}, G_{k,n}, M_{k,n}) \approx 0.2 \exp\left\{ -\frac{m\left(M_{k,n}\right)}{2\left(M_{k,n}-1\right)} \frac{G_{k,n}}{\sigma_W^2} |H_{k,n}|^2 \right\} \tag{54}$$

where the function $m(M_{k,n})$ depends on the size/type of the modulation $M_{k,n}$. These coefficients are achieved numerically for each modulation type/size based on the BER approximation which is obtained by fitting (54) to original BER curves. We assign the highest modulation on each subcarrier in a manner not to exceed the target BER on that subcarrier.

Although this scheme is adaptive and results in higher data rates with respect to non-adaptive scheme, it is not optimum because some of subcarriers could accept higher modulation. This might exceed targeted BER on the subcarrier while the average BER might be still be less or equal to target BER. With this motivation in mind, we also propose the following scheme for bit loading.

Adaptive Algorithm 2: In this algorithm, we modify the previous maximization problem as

$$\begin{aligned} &\max_{M_{0,n},\ldots,M_{K-1,n}} \sum_{k=0}^{K-1} \log_2 M_{k,n} \\ &subject\,to: \ \tfrac{1}{K}\sum_{k=0}^{K-1} P_{e,k} = P_b \\ &G_{k,n} = \tfrac{1}{K} G_n \end{aligned} \tag{55}$$

In this case, the average BER is important and the bit loading is done in a way to maximize throughput while satisfying a targeted average BER. We employ a greedy algorithm which calculates the modulation size/type for the n-th block considering the allocations from the last block for the first step [39], [42], [43]. After first allocation, we increase the modulation levels for those subcarriers that require the minimum BER increment, while keeping the average BER below the target P_b. If it fails during the initial step, it looks for the subcarrier with the highest BER decrement that is needed in order to decay the modulation size/type. The algorithm is stopped when the target BER is achieved.

Adaptive Algorithm 3: In the previous algorithms, we consider adaptive allocation of the modulation levels to each subcarrier while the total power is equally distributed across subcarriers. However in this algorithm, adaptive allocation of the modulation levels and the sub-carrier powers are done such that $P_{e,k} = P_b$. Therefore the optimization problem is rewritten as:

$$\begin{aligned} &\max_{M_{0,n},\ldots,M_{K-1,n}} \sum_{k=0}^{K-1} \log_2 M_{k,n} \\ &subject\,to: \sum_{k=0}^{K-1} G_{k,n} = G_n \\ &P_{e,k} = P_e \end{aligned} \tag{56}$$

We use (3) to define $G_{n,k}$ as a function of $P_{e,k}$ to obtain power thresholds on each subcarriers, i.e.,

$$G_{k,n}(H_{k,n}, P_{e,k}, M_{k,n}) \approx \frac{-2\sigma_W^2 \left(M_{k,n} - 1\right)}{m\left(M_{k,n}\right) \left|H_{k,n}\right|^2} \ln\left(5P_{e,k}\right) \tag{57}$$

Similar to the previous one, greedy algorithm is used to allocate modulation and power level. After initial allocation, we look for the subcarrier k^* with the smallest power increment that is required in order to increase the modulation level $M_{k^*,n}$. If the algorithm fails during the initial step, it searches for the subcarrier k^* with the highest decrease in power that is required in order to decrease the modulation level

$M_{k^*,n}$. For those subcarriers which facing deep fade, no data will be transmitted (zero power allocation). The algorithm is stopped when the total power G_n is exceeded, or when all subcarriers achieve the maximum modulation level (16-QAM).

4.2 Simulation results

In the following, we present performance results for the three adaptive OFDM algorithms described above. The channel impulse response (CIR) used in the simulations is provided in Fig 70. The system parameters are summarized in Table 3.

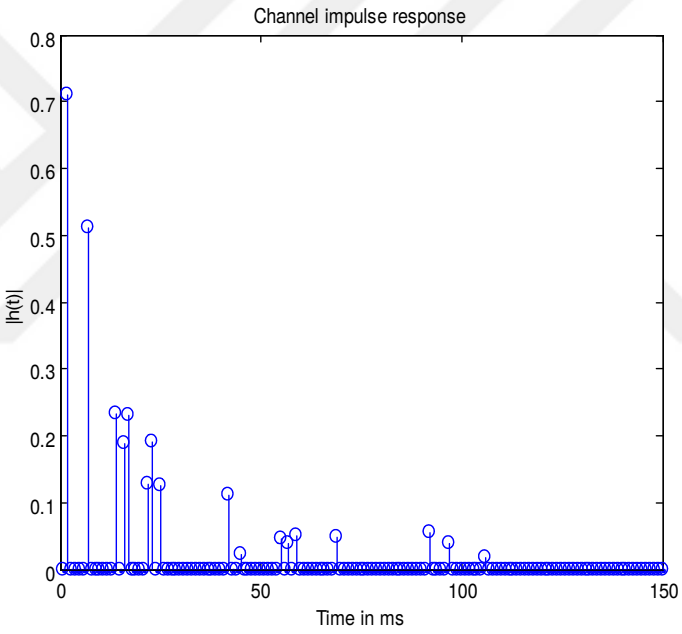

Figure 70: Channel impulse response

In Fig 71, we consider Adaptive Algorithm 1. BER per subcarrier is shown for different modulations versus subcarrier indexes from $k = 80$ to $k = 100$. Overall power is $G_n = 40dB$ while the targeted value of BER is $P_b = 10^{-3}$. In this algorithm, we select the best modulation on each subcarrier which does not exceed the targeted BER. Selected modulation on each subcarrier is shown by circle. It can be noticed that some subcarriers cannot satisfy the threshold for any modulation, e.g. $k = 86, 87$, and no data is transmitted on those subcarriers.

Table 3: Adaptive system parameters

Parameters	values
Number of Subcarriers	$K = 1024$
OFDM block duration	$T = 85.33ms$
Guard interval	$T_g = 10ms$
Signal Bandwidth	$B = 12kHz$
Modulation	BPSK/QPSK/8PSK
Pulse shaping	Raised-Cosine ($\beta = 0.5$)

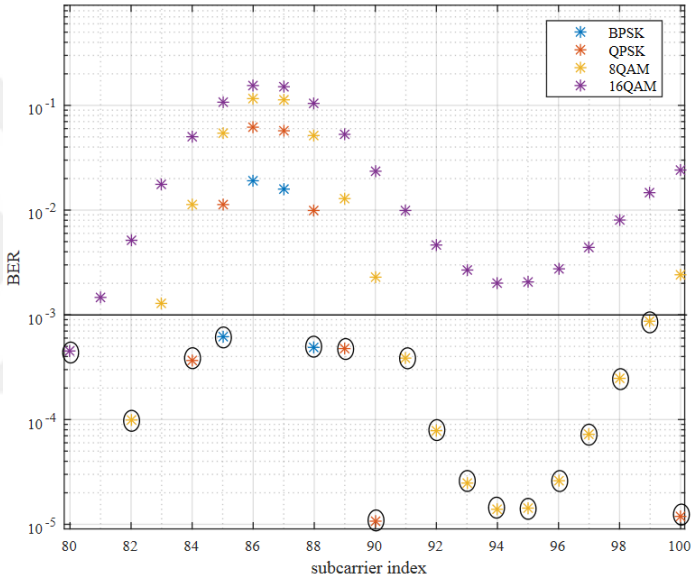

Figure 71: BER versus subcarrier index for different modulations

In Fig 72, we consider Adaptive Algorithm 2 and illustrate modulation levels across the data subcarriers for a specific OFDM symbol with overall power of 40dB. The targeted average BER is $P_b = 10^{-3}$. As it is shown different subcarriers accept different levels of modulation regarding their channel state.

In Fig 73, we consider Adaptive Algorithm 3 and illustrate the allocated power across the data subcarriers for an arbitrary OFDM symbol with overall power of 40 dB. The targeted fixed BER per subcarrier is $P_b = 10^{-3}$. It is observed that different subcarriers accept different levels of power regarding their channel state.

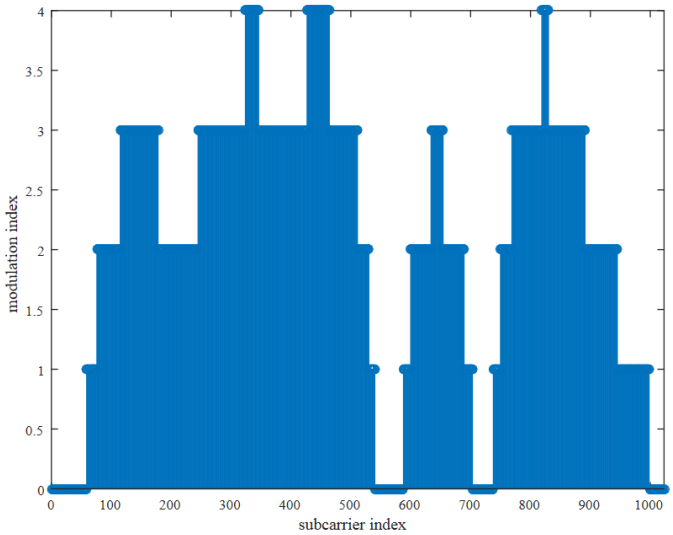

Figure 72: Modulation levels across the subcarriers for Adaptive Algorithm 2

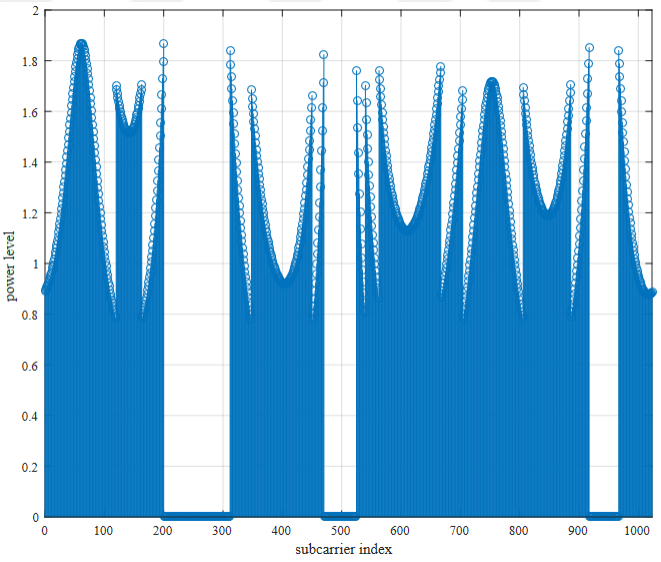

Figure 73: Allocated power levels across the subcarriers for Adaptive Algorithm 3

In Fig 74, we compare the throughput of three adaptive algorithms under consideration for a fixed BER ($P_b = 10^{-3}$). Due to additional freedom of adopting the transmit power, the third scheme achieves a higher throughput. The second best performance belongs to Adaptive Algorithm 2.

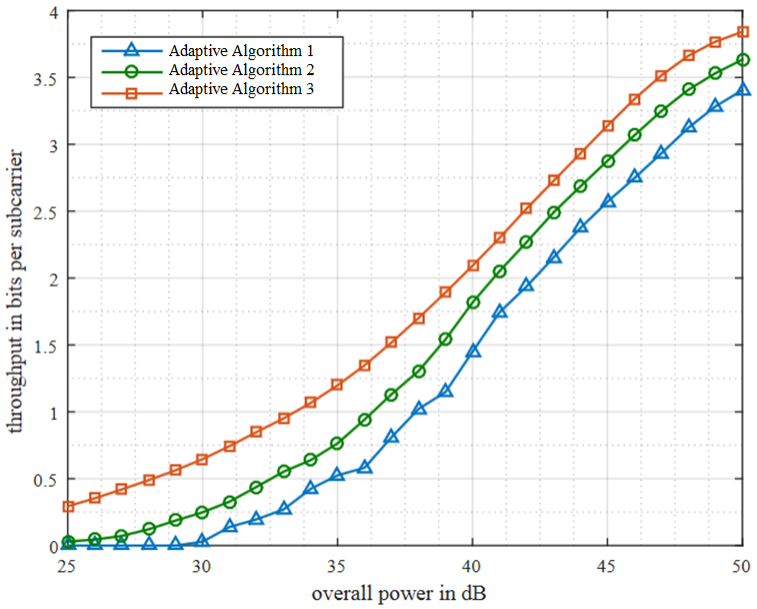

Figure 74: Throughput comparison of three adaptive algorithms

4.3 Adaptive system implementation

In this section, we present the implementation of an adaptive OFDM-based software defined modem using Labview and National Instrument USRPs. The general block diagram of the adaptive system under consideration is illustrated in Fig 75.

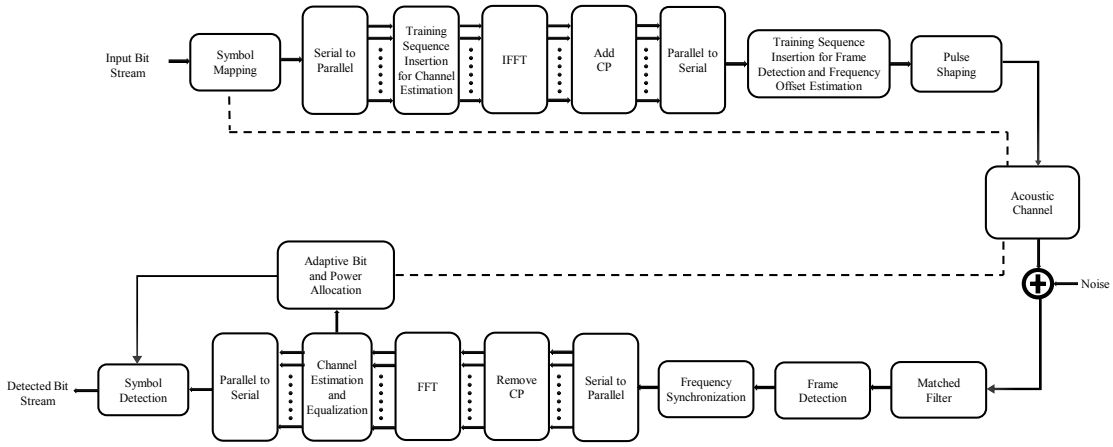

Figure 75: System overview

In this system, first, transmitter sends a known pilot stream to the receiver side to estimate the channel condition. At the receiver side the pilot stream is extracted and

the adaptive metrics (modulation size and power level on each subcarrier) are calculated in the adaptive blocks. Then, the adaptive metrics are fed back to transmitter side. The received adaptive metric at the transmitter side are demodulated and the modulation sizes and power levels are assigned to subcarriers according to received feedback. Finally, information data is transmitted to the receiver in the adaptive mode. Therefore we have three stages for transmission. In all stages we consider an OFDM system with K subcarriers. The input bit stream is first mapped to the modulation symbols according to received feedback or fixed modulation for feedback data transmission. The adopted modulations are BPSK, 4-QAM, 8-QAM and 16-QAM. For the transmission purpose, K-point IFFT is applied and a CP is appended to eliminate the ISI caused by multipath effect. Additionally, two training sequences and a guard interval are added at the beginning of each OFDM frame for frame detection, frequency offset estimation and separation of frames respectively. For the receiver purposes at both sides, the correlation properties of the known training sequences are used for frame detection and frequency synchronization. Schmidl-Cox algorithm is applied for frequency synchronization. Each OFDM frame is then partitioned into individual OFDM symbols. After CP elimination, the resulting sequence is applied to FFT. Afterwards, channel estimation and one tap equalizer are performed. Finally, the equalized data symbols are demodulated and the information data is recovered (details about OFDM implementation are provided in chapter 3). In the following we explain these stages with more details.

First Stage: In the first stage, to overcome the time-varying nature of underwater channel, a known training pilot streams are arranged in the block type form. In block type channel estimation, pilot symbols are transmitted periodically in which all subcarriers are used as pilots. If the channel remains fixed during one block, there will be error free channel estimation, since the pilots are used at all subcarrier. In the receiver side, the known pilot symbols are extracted for channel estimation

and consequently computing the adaptive metrics (modulation size and power level of each subcarrier) for adaptive data transmission. The estimation performed by using Least Square (LS). The estimated channel is used to compute adaptive metrics with three different adaptive which are introduced in chapter 4. In the first and the second scheme, bit allocation (through the choice of proper modulation sizes) is made adaptively to each subcarrier and the power is equally distributed among subcarriers. The third scheme allocates both modulation and power adaptively based on the channel state information at the subcarrier. Each algorithm is explained in more details in the previous section.

Second Stage: In this stage, we transmit the computed modulation sizes and the quantized power levels assigned to each subcarrier directly to the transmitter using OFDM technique with fixed coding and modulation, i.e., convolutional code and QPSK modulation. We use three bits to present 5 modulation levels and the constructed bits stream is then encoded by convolutional coding and mapped to QPSK symbols. The power levels are first normalized to total power and then uniformly quantized to 16 quantization levels which are represented with four bits, then encoded by convolutional coding and mapped to QPSK symbols.

At the transmitter side, we use the fixed OFDM receiver to process and demodulate the feedback signals.

Third Stage: In this stage at the transmitter side, the decoded indices stream, i.e., modulation on each subcarrier, is provided as an input for modulation block. The modulation block separates information bits and maps them to symbols according to the indices vector.

At the receiver side, the received data will be demodulated based on the same indices calculated at first stage in the receiver and forwarded to this stage. Finally, demodulated bits are compared with original bit streams and the bit error rate is obtained.

4.4 Experimental results

In this section, we present the real-time experimental results obtained from pool trials at SUASIS company to evaluate the performance of the designed system. The transmitter and receiver are submerged in the pool at a depth of 2 meters. The distance between transmitter and receiver is varied between 0.5 to 2 meters. The system parameters are summarized in Table 4.

Table 4: System parameters

Parameters	**Values**
Number of Subcarriers	$K = 64, 128$
Carrier Frequency	30 KHz
Modulation	BPSK/ 4-QAM/ 8-QAM/ 16-QAM
Pulse Shaping	Raised cosine ($\beta = 0.5$)
Bandwidth	4 KHZ
Guard Time	15 ms
Feedback Length	$3, 7$ OFDM symbols

In Fig 76.a, we demonstrate the loaded bits on each subcarrier for a specific OFDM symbol with 64 subcarriers at the approximate transmit power of 24dB and the distance of 0.5 meter. The target average BER is 0.05. It can be noticed that algorithm 3 achieves higher modulation sizes compared to other algorithms as a result of power adaptation. In Fig 77.b, to evaluate our system for a range of SNRs, we show average achievable throughput (in bits per subcarrier) results for the designed OFDM systems with the same parameters considered in Fig 77.a. It is demonstrated that algorithm 3 outperforms algorithm 2 for the considered range of SNRs. This outperformance decreases as the average SNR increases, since algorithm 3 tends to distribute power among subcarriers more equally in large SNRs regime which makes source to transmit more similar to algorithm 2. Additionally, note that adapting both modulation and power incurs more feedback loads.

In Fig 77, we repeated the throughput test at the distance of 1 with 128 subcarriers with the target average BER of 0.05. It can be noticed that scheme 3 achieves higher modulation due to its ability to adapt power on each subcarrier. Comparing to the previous results, it can be observed that the system achieve lower throughputs as the

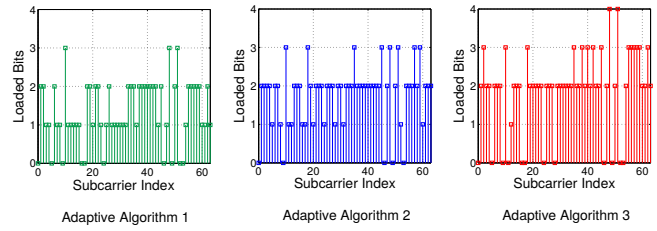

(a)

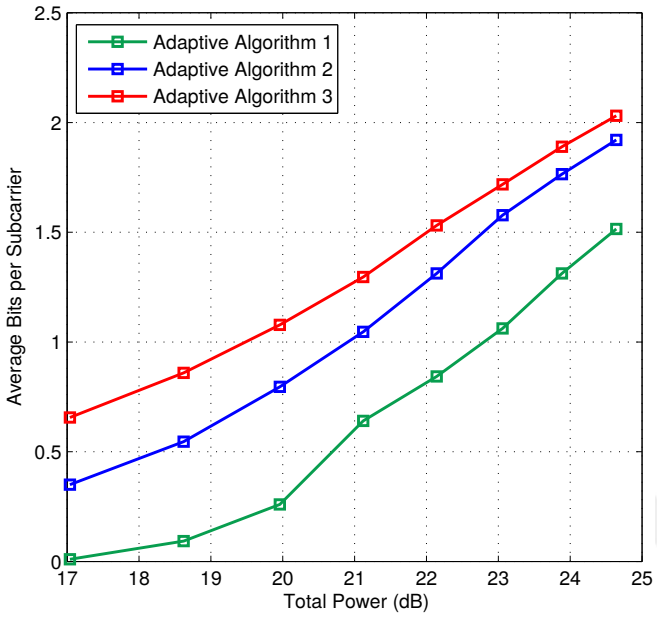

(b)

Figure 76: (a) Loaded bits on each subcarrier for Adaptive Algorithm 1, 2 and 3. (b) Average bits per subcarrier versus total transmitted power in dB

distance increases due to higher attenuation and more severe multipath effects.

We compared the BER in same scenario with fixed 4-QAM modulation for 15 consecutive packets in Fig 78. It is shown that unlike fixed scheme, in adaptive algorithm subcarrier can accept different modulation with relatively lower BER.

The averages bits per subcarrier versus distances of 0.5 to 2 meters are depicted in Fig 79 at the approximate transmit power of 26 dB. It can be noticed that the achieved throughput decreases as the distance increases due to attenuation and more severe multipath effects.

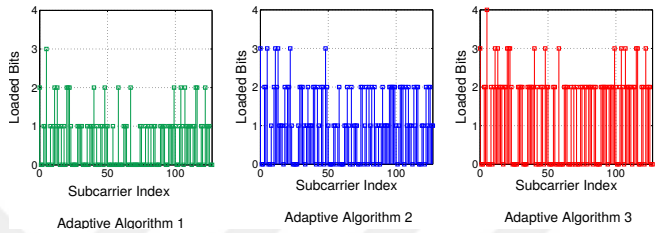

(a)

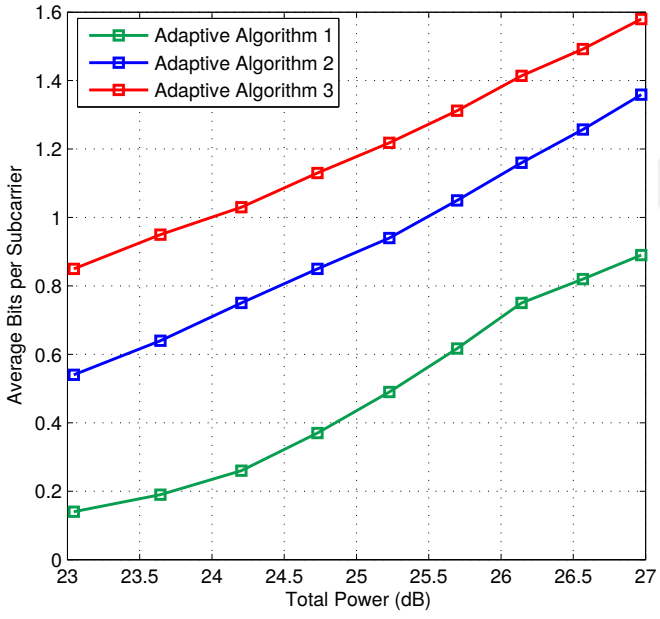

(b)

Figure 77: (a) Loaded bits on each subcarrier for Adaptive Algorithm 1, 2 and 3. (b) Average bits per subcarrier versus total transmitted power in dB

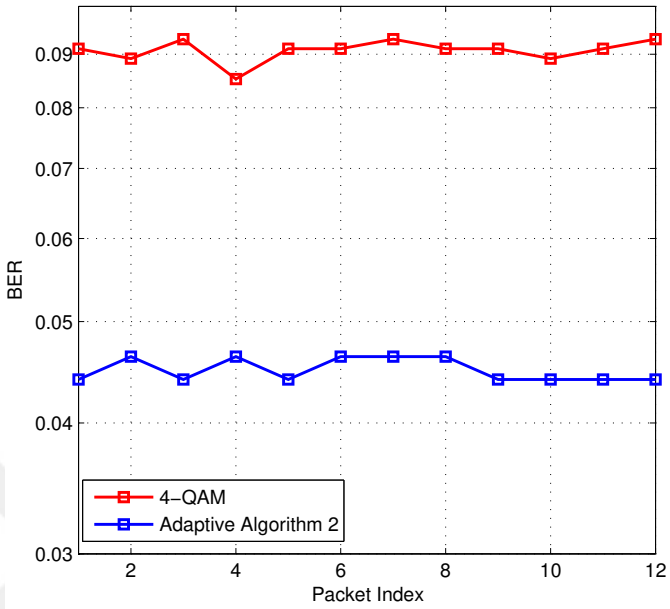

Figure 78: BER comparison of fixed and Adaptive Algorithm 2

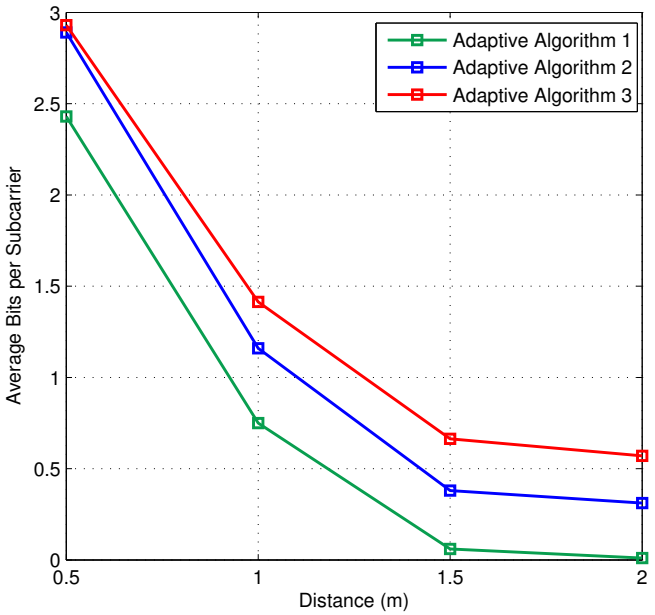

Figure 79: Average bits per subcarrier versus distance at the transmit power of 26 dB

CHAPTER V

CONCLUSIONS

We designed and implemented a custom OFDM based software defined UWA modem that adapted modulation and the transmit power on each subcarrier to maximize system throughput while maintain the BER at the specified threshold. Three different adaptive schemes are employed where in the first and second schemes only the modulation is adapted across subcarrier and the total power is equally distributed among the subcarriers, while in the third scheme, both modulation and power are adapted. The experimental results showed that, scheme 3 achieves a highest throughput due to additional freedom of adapting the transmit power. The second best performance belongs to adaptive algorithm 2. We conducted the underwater trials in the pool to evaluate the performance of the designed system.

Bibliography

[1] M. Stojanovic, J. Catipovic, and J. Proakis, "Phasecoherent digital communications for underwater acoustic channels," *IEEE J. Ocean. Eng*, vol. 19, pp. 100–111, Jan. 1994.

[2] W. Li and J. C. Preisig, "Estimation of rapidly time-varying sparse channels," *IEEE Journal of Oceanic Engineering*, vol. 32, pp. 927–939, Oct 2007.

[3] S. Roy, T. M. Duman, V. McDonald, and J. G. Proakis, "High-rate communication for underwater acoustic channels using multiple transmitters and space x2013;time coding: Receiver structures and experimental results," *IEEE Journal of Oceanic Engineering*, vol. 32, pp. 663–688, July 2007.

[4] D. B. Kilfoyle, J. C. Preisig, and A. B. Baggeroer, "Spatial modulation over partially coherent multiple-input/multiple-output channels," *IEEE Transactions on Signal Processing*, vol. 51, pp. 794–804, March 2003.

[5] D. B. Kilfoyle, J. C. Preisig, and A. B. Baggeroer, "Spatial modulation experiments in the underwater acoustic channel," *IEEE Journal of Oceanic Engineering*, vol. 30, pp. 406–415, April 2005.

[6] S. Roy, T. M. Duman, V. McDonald, and J. G. Proakis, "High-rate communication for underwater acoustic channels using multiple transmitters and space x2013;time coding: Receiver structures and experimental results," *IEEE Journal of Oceanic Engineering*, vol. 32, pp. 663–688, July 2007.

[7] M. Stojanovic and Z. Zvonar, "Multichannel processing of broad-band multiuser communication signals in shallow water acoustic channels," *IEEE Journal of Oceanic Engineering*, vol. 21, pp. 156–166, Apr 1996.

[8] A. Song and M. Badiey, "Time reversal multiple-input/multiple-output acoustic communication enhanced by parallel interference cancellation," *Journal of Acoustical Society of America*, vol. 131, pp. 281–291, Jan 2012.

[9] A. Song, M. Badiey, V. K. McDonald, and T. C. Yang, "Time reversal receivers for high data rate acoustic multiple-input x2013;multiple-output communication," *IEEE Journal of Oceanic Engineering*, vol. 36, pp. 525–538, Oct 2011.

[10] H. C. Song, W. S. Hodgkiss, W. A. Kuperman, T. Akal, and M. Stevenson, "Multiuser communications using passive time reversal," *IEEE Journal of Oceanic Engineering*, vol. 32, pp. 915–926, Oct 2007.

[11] H. C. Song, P. Roux, W. S. Hodgkiss, W. A. Kuperman, T. Akal, and M. Stevenson, "Multiple-input-multiple-output coherent time reversal communications in a shallow-water acoustic channel," *IEEE Journal of Oceanic Engineering*, vol. 31, pp. 170–178, Jan 2006.

[12] J. Zhang and Y. R. Zheng, "Bandwidth-effiient frequency-domain equalization for single carrier multiple-input multiple-output underwater acoustic communications," *Journal of Acoustical Society of America*, vol. 128, pp. 2910–2919, Nov 2010.

[13] J. Zhang and Y. R. Zheng, "Frequency-domain turbo equalization with soft successive interference cancellation for single carrier mimo underwater acoustic communications," *IEEE Transactions on Wireless Communications*, vol. 10, pp. 2872–2882, September 2011.

[14] J. Ling, X. Tan, T. Yardibi, J. Li, M. L. Nordenvaad, H. He, and K. Zhao, "On bayesian channel estimation and fft-based symbol detection in mimo underwater acoustic communications," *IEEE Journal of Oceanic Engineering*, vol. 39, pp. 59–73, Jan 2014.

[15] J. Ling, T. Yardibi, X. Su, H. He, and J. Lia, "Enhanced channel estimation and symbol detection for high speed multi-input multi-output underwater acoustic communications," *Journal of Acoustical Society of America*, vol. 59, pp. 3067–3078, May 2009.

[16] A. Rafati, H. Lou, and C. Xiao, "Soft-decision feedback turbo equalization for ldpc-coded mimo underwater acoustic communications," *IEEE Journal of Oceanic Engineering*, vol. 39, pp. 9.–99, Jan 2014.

[17] J. Tao, J. Wu, Y. R. Zheng, and C. Xiao, "Enhanced mimo lmmse turbo equalization: Algorithm, simulations, and undersea experimental results," *IEEE Transactions on Signal Processing*, vol. 59, pp. 3813–3823, Aug 2011.

[18] J. Tao, Y. R. Zheng, C. Xiao, and T. C. Yang, "Robust mimo underwater acoustic communications using turbo block decision-feedback equalization," *IEEE Journal of Oceanic Engineering*, vol. 35, pp. 948–960, Oct 2010.

[19] L. Wang, J. Tao, C. Xiao, and T. Yang, "Low-complexity turbo detection for single-carrier ldpc coded mimo underwater acoustic communications," *Wireless Communications and Mobile Computing*, vol. 13, pp. 439–450, Mar 2013.

[20] L. Wang, J. Tao, and Y. Zheng, "Single-carrier frequency-domain turbo equalization without cyclic prefix or zero padding for underwater acoustic communications," *Journal of Acoustical Society of America*, vol. 132, pp. 3809–3817, Dec 2012.

[21] J. Huang, J.-Z. Huang, C. R. Berger, S. Zhou, , and P. Willett, "Iterative sparse channel estimation and decoding for underwater mimo-ofdm," *EURASIP Journal on Advances in Signal Processing*, 2010.

[22] J. Huang, S. Zhou, J. Huang, J. Preisig, L. Freitag, and P. Willett, "Progressive intercarrier and co-channel interference mitigation for underwater acoustic mimo-ofdm," *Wireless Communications and Mobile Computing*, Feb 2012.

[23] B. Li, J. Huang, S. Zhou, K. Ball, M. Stojanovic, L. Freitag, and P. Willett, "Mimo-ofdm for high-rate underwater acoustic communications," *IEEE Journal of Oceanic Engineering*, vol. 34, pp. 634–644, Oct 2009.

[24] P. C. Carrascosa and M. Stojanovic, "Adaptive channel estimation and data detection for underwater acoustic mimo x2013;ofdm systems," *IEEE Journal of Oceanic Engineering*, vol. 35, pp. 635–646, July 2010.

[25] M. Stojanovic, "Mimo ofdm over underwater acoustic channels," in *2009 Conference Record of the Forty-Third Asilomar Conference on Signals, Systems and Computers*, pp. 605–609, Nov 2009.

[26] "Cylindrical vs. spherical spreading," *Discovery of Sound in the Sea, [Online]. Available: http://www.dosits.org/science/advancedtopics/spreading/*.

[27] A. Sehgal, "Analysis simulation of the deep sea acoustic channel for sensor networks," *Bremen: Jacobs University, School of Engineering and Science*, Aug 2009.

[28] S. Aldharrab, "Cooperative communication over underwater acoustic channels," *Ontario: Waterloo, Canada*, 2013.

[29] S. Zhou and Z. Wang, "Ofdm for underwater acoustic communications," *John Wiley Sons*, 2014.

[30] M. Chitre, "A high-frequency warm shallow water acoustic communications channel," *Acoustic Research Laboratory, National University of Singapore*, vol. 122, pp. 2580–2586, Nov 2007.

[31] D. Jourdain, "High frequency signal fluctuation in shallow water propagation," in *Proc. IEEE Oceans'94 Conf-Brest, France*, Sep 1994.

[32] T. Yang, "Characterization and modeling of underwater acoustic communications channels for frequency-shift-keying signals," in *Naval Research Laboratory, Washington, DC 20375 USA*, pp. 1–6, Sep 2006.

[33] X. Lurton, "Introduction to underwater acoustics: Principles and applications," *New York*, 2002.

[34] K. Prasanth, "Modelling and simulation of an underwater acoustic communication channel," *Bremen: University of applied sciences*.

[35] A. J. Goldsmith and S.-G. Chua, "Variable-rate variable-power mqam for fading channels," *IEEE Transactions on Communications*, vol. 45, pp. 1218–1230, Oct 1997.

[36] D. L. Goeckel, "Adaptive coding for time-varying channels using outdated fading estimates," *IEEE Transactions on Communications*, vol. 47, pp. 844–855, Jun 1999.

[37] T. Keller and L. Hanzo, "Adaptive multicarrier modulation: a convenient framework for time-frequency processing in wireless communications," *Proceedings of the IEEE*, vol. 88, pp. 611–640, May 2000.

[38] P. Qarabaqi and M. Stojanovic, "Adaptive power control for underwater acoustic communications," in *OCEANS 2011 IEEE - Spain*, pp. 1–7, June 2011.

[39] A. Radosevic, R. Ahmed, T. M. Duman, J. G. Proakis, and M. Stojanovic, "Adaptive ofdm modulation for underwater acoustic communications: Design considerations and experimental results," *IEEE Journal of Oceanic Engineering*, vol. 39, pp. 357–370, April 2014.

[40] A. Radosevic, R. Ahmed, T. M. Duman, J. G. Proakis, and M. Stojanovic, "Adaptive ofdm modulation for underwater acoustic communications: Design considerations and experimental results," *IEEE Journal of Oceanic Engineering*, vol. 39, pp. 357–370, April 2014.

[41] E. Demirors, G. Sklivanitis, G. Santagati, and T. Melodia, "Design of a software-defined underwater acoustic modem with real-time physical layer adaptation capabilities," in *Proceedings of the International Conference on Underwater Networks Systems*, vol. 1, p. 24, Nov 2014.

[42] R. F. H. Fischer and J. B. Huber, "A new loading algorithm for discrete multitone transmission," in *Global Telecommunications Conference, 1996. GLOBECOM '96. 'Communications: The Key to Global Prosperity*, vol. 1, pp. 724–728 vol.1, Nov 1996.

[43] J. Campello, "Practical bit loading for dmt," in *1999 IEEE International Conference on Communications (Cat. No. 99CH36311)*, vol. 2, pp. 801–805 vol.2, 1999.

VITA

Mohammad Sadeghi received his B.Sc. degree in electrical engineering from University of Isfahan, Isfahan, Iran, in 2015. He was a M.Sc. student at Electrical and Electronic engineering department and a member of Communication Theory and Technology (CT&T) research group under supervision of Professor Murat Uysal at Ozyegin University, Istanbul, Turkey. His research is in the area of OFDM systems, Underwater acoustic communications and cooperative communications.